Remote Sensing of Environment 179 (2016) 89–103

Contents lists available at ScienceDirect

Remote Sensing of Environment

journal homepage: www.elsevier.com/locate/rse

Seasonal stability of chlorophyll fluorescence quantified from airborne hyperspectral imagery as an indicator of net photosynthesis in the context of precision agriculture

P.J. Zarco-Tejada [a,*], M.V. González-Dugo [a], E. Fereres [a,b]

[a] Instituto de Agricultura Sostenible (IAS), Consejo Superior de Investigaciones Científicas (CSIC), Alameda del Obispo s/n, 14004 Córdoba, Spain
[b] Departamento de Agronomía, Universidad de Córdoba, Campus Universitario de Rabanales, 14014 Córdoba, Spain

ARTICLE INFO

Article history:
Received 17 September 2015
Received in revised form 10 March 2016
Accepted 23 March 2016
Available online xxxx

Keywords:
Hyperspectral
Fluorescence
SIF
FLD
In-filling
Photosynthesis
Airborne
Stress detection

ABSTRACT

The seasonal stability of solar-induced chlorophyll fluorescence (SIF) vs field-measured leaf CO_2 assimilation (A) was assessed over a period of 2 years by means of airborne flights performed at midday and diurnally over a citrus (evergreen) crop canopy. The orchard was cultivated under a control treatment (ET) that received 100% of its water requirements and two regulated deficit irrigation (RDI) treatments with water supply reduced to 37% and 50% of the control level during the summer. Field measurements consisted of assimilation rate, stomatal conductance, stem water potential, leaf fluorescence and leaf reflectance. The airborne campaigns took place in 2012 and 2013, and were flown on the solar plane in order to acquire hyperspectral imagery at 40 cm resolution, 260 spectral bands and 1.85 nm/pixels in the 400–885 nm spectral region. A thermal camera was installed in tandem in all flights, acquiring imagery in the 7.5–13 μm spectral region at 640 × 480 pixel resolution, yielding a 50 cm pixel size. The robustness of the SIF quantification through the Fraunhofer Line Depth (FLD) principle based on three spectral bands (FLD3), as well as the performance of physiological and structural hyperspectral indices, was evaluated in order to understand their ability to track photosynthesis at different phenological and stress stages throughout the season. Solar induced fluorescence quantified as FLD3 was the most robust indicator of photosynthesis in all the airborne campaigns performed in the course of the two-year experiment, which comprised seven midday flights and two diurnals. The relationships between fluorescence (FLD3) and assimilation rates yielded correlation coefficients (R) between 0.64 and 0.82 across all dates, these being statistically significant with *p*-values between $p < 0.05$ and $p < 0.0001$. Fluorescence retrievals performed better than structural and physiological indices, with the structural MTVI1 index being the only other statistically significant indicator throughout the season, although it yielded lower levels of significance than FLD3. A normalization strategy proposed for SIF FLD3 for all dates using control (ET) trees on each flight date as a reference permitted the generation of a single relationship between FLD3 normalized (FLDn) and assimilation rates for the entire year, both at tree ($r^2 = 0.5$; $p < 0.0001$) and treatment level ($r^2 = 0.72$; $p < 0.0001$), a strategy that confirmed the ability of seasonal SIF retrievals to track photosynthesis from broader resolution hyperspectral imagery (i.e. spectral resolution 1–5 nm full-width at half maximum (FWHM)) for applications in the context of precision agriculture and crop-monitoring studies.

1. Introduction

Rising attention is being paid to solar-induced chlorophyll fluorescence (SIF) for global assessment of vegetation physiology, particularly as a means of monitoring crop photosynthesis on global scales (Guanter et al., 2014). Such worldwide interest in chlorophyll fluorescence is partly due to the need to improve the inputs and methods used in current carbon-cycle models for global estimates of gross primary production (GPP), which in some cases have produced large errors with results that differ by a factor of two compared to tower-flux data networks (Schaefer et al., 2012). The best estimates of the GPP of crop systems are widely accepted to be derived from direct measurement of carbon dioxide exchange by flux towers (Baldocchi et al., 2001) but these tend to sample small areas and are spatially scattered. Image-based remote quantification of SIF, emitted in the 650–850 nm region of the spectrum as a by-product of photosynthesis (Porcar-Castell et al., 2014; Meroni et al., 2009; Rascher et al., 2009), is therefore regarded as critical, as it has been proposed as a direct proxy for photosynthetic rate and related to vegetation stress conditions. Although the rise in interest is very recent, studies carried out around the end of the last century had already demonstrated the links between chlorophyll fluorescence

* Corresponding author.
E-mail address: pablo.zarco@csic.es (P.J. Zarco-Tejada).
URL: http://quantalab.ias.csic.es (P.J. Zarco-Tejada).

http://dx.doi.org/10.1016/j.rse.2016.03.024
0034-4257/

emission and photosynthesis (Papageorgiou, 1975; Krause & Weis, 1984; Schreiber & Bilger, 1987; Lichtenthaler & Rinderle, 1988; Lichtenthaler, 1992; Larcher, 1994; Schreiber, Bilger, & Neubauer, 1994), with most of the fluorescence quantification efforts being performed later at leaf and near-canopy levels (Pérez-Priego, Zarco-Tejada, Sepulcre-Cantó, Miller, & Fereres, 2005; Meroni, Colombo, & Cogliati, 2004, 2008a, 2008b, 2009, Moya et al., 2004; Cogliati et al., 2015). Specifically, some studies have focused on the technical side of the fluorescence quantification for monitoring global photosynthesis (Malenovsky, Mishra, Zemek, Rascher, & Nebal, 2009) or on leaf- to regional-level scaling issues using the O_2 bands (Rascher et al., 2009), in addition to modelling GPP from fluorescence/assimilation rates in diurnal patterns (Damm et al., 2010).

Besides the methodological advances in chlorophyll fluorescence emission retrieval, efforts to assess crop physiology from remote sensing have focused on the development of new indicators calculated from hyperspectral reflectance imagery based on narrow spectral bands related to canopy structure and photosynthetic pigments, including chlorophyll, xanthophylls and carotenoids (Quemada, Gabriel, & Zarco-Tejada, 2014; Hernandez-Clemente et al., 2014; Zarco-Tejada et al., 2013a). The interest in the development of these reflectance-based physiological indices relies on the fact that traditional vegetation indices such as the Normalized Difference Vegetation Index (NDVI) are highly sensitive to the phenology that usually drives the main structural changes that occur throughout the season, being saturated at larger leaf-area index values (Haboudane et al., 2004) and masking smaller physiological variations due to water or nutrient availability (Suárez et al., 2008; Suárez, Zarco-Tejada, Berni, González-Dugo, & Fereres, 2009). Among the proposed physiological indices, the Photochemical Reflectance Index (PRI) (Gamon, Peñuelas, & Field, 1992) has been suggested as a proxy for photosynthesis, demonstrating its dynamic changes along with photosynthesis in different vegetation canopies, including grapevines (Evain, Flexas, & Moya, 2004), Scots pine (Louis et al., 2005), experimental mangrove canopies (Nichol, Rascher, Matsubara, & Osmond, 2006) and coastal shrubs (Naumann, Young, & Anderson, 2008). Before these reflectance-based hyperspectral indices and fluorescence emission quantities can be readily applied on larger scales, a better understanding of fluorescence emission and the interpretation of physiological changes at different stress levels and spatial resolutions is necessary (Zarco-Tejada et al., 2013b); this is particularly important in the context of precision agriculture and decision-making to improve fruit quality and yields, and to reduce water and fertilizer use. In this context of water-stress detection and precision irrigation, seasonal monitoring of fluorescence from airborne imagery has demonstrated a link with assimilation rates in crops with little structural changes over the growing season (Zarco-Tejada, González Dugo, & Berni, 2012, 2013c), and for disease detection at pre-visual stages, using airborne-retrieved fluorescence data derived from high-resolution hyperspectral imagery (Calderon et al., 2013, 2015).

On the modelling side, important progress has been made since the first attempts as part of FluorMOD (Miller et al., 2004) with recent developments and updates on the integrated leaf-canopy fluorescence-temperature-photosynthesis model (SCOPE) (Van der Tol et al., 2009a, 2009b), used to assess the key variables that drive (SIF) from vegetation canopies (Verrelst et al., 2015) in the context of the FLuorescence EXplorer FLEX mission supported by the European Space Agency (ESA) Earth Explorer program. However, the large number of inputs required makes its direct application difficult outside of experimental studies, which thus imposes important limitations on its use for operational purposes in commercial orchards and precision agriculture applications. Regarding the imaging sensors available for fluorescence quantification, current state-of-the-art methodologies for fluorescence retrieval are based on sub-nanometer spectral resolution of hyperspectral data at both leaf and canopy levels. Nevertheless, actual access to very high spectral resolution imagery is still quite limited (e.g. HyPlant, an airborne sensor designed to cover the 670 to 780 nm region with 0.25 nm FWHM bands and 0.11 nm sampling interval), as these sensors are only available for scientific purposes and have demonstrated successful retrievals of fluorescence linked to photosynthetic efficiency (Rossini et al., 2015). Despite such *standard* sensor specifications and narrow-band requirements, recent studies have demonstrated that hyperspectral imagery acquired at 5–6 nm FWHM and long sampling intervals is capable of retrieving fluorescence with relatively high success. This has been demonstrated through modelling (Damm et al., 2011) and in experimental studies which displayed relationships with field-measured assimilation and fluorescence levels (Zarco-Tejada, Catalina, González, & Martín, 2013d), carbon data measured from a flux tower (Zarco-Tejada et al., 2013c), and ecosystem-specific fluorescence retrievals linked to gross primary production using the Airborne Prism EXperiment (APEX) characterized by a spectral sampling interval of 4.5 nm and a FWHM of 5.7 nm (Damm et al., 2015). The theoretical and experimental results obtained using broader bandwidths (i.e. FWHM > 1 nm) are of paramount importance for the operational and widespread application of chlorophyll fluorescence retrievals and hyperspectral indices for monitoring physiological status using commercially available sensors in the context of precision agriculture, plant phenotyping, precision forestry and disease detection. For some of these purposes, the actual retrieval of the fluorescence quantification in absolute terms is not absolutely critical, while the spatial variability (i.e. relative differences among stress levels, treatments and disease affection) is the important factor for precision agriculture and stress-detection purposes in an operational context (see Zarco-Tejada et al., 2012 for a demonstration of fluorescence retrievals for stress-detection purposes using a micro-hyperspectral imager carried on board an unmanned aerial vehicle). Nevertheless, the impact of fluorescence retrieval errors when using broader spectral bands (i.e. FWHM > 1 nm) is unknown in the context of seasonal studies performed for agronomic and stress detection purposes, and for the assessment of the temporal relationships between photosynthesis rates and fluorescence quantification measured under different irradiance levels and atmospheric conditions.

In this study we assess the stability of the fluorescence quantification over a two-year period of hyperspectral flights as compared to field-measured leaf assimilation in an evergreen crop canopy (orange) grown under different water stress levels. We evaluate the robustness of the fluorescence quantification and physiological and structural indices in order to understand their ability to track photosynthesis at different phenological and stress stages throughout the season, and suggest taking a fluorescence normalization approach to its operational use in precision agriculture.

2. Materials and methods

2.1. Field experiments and airborne campaigns

2.1.1. Study site and field data collection

The experiment was carried out in a commercial orange (*Citrus sinensis* L. cv. Powell) grove near La Campana, Seville (Spain (37.8°N, 5.4°W) in 2012 and 2013. The orchard was planted in 1997 in a 7×4 m grid on a deep alluvial loamy to sandy loam soil. For further information regarding the experimental set-up and local climate characteristics, see Zarco-Tejada et al. (2012). Three irrigation treatments were applied: a control treatment (ET), that received 100% of the estimated crop evapotranspiration and was never short of water, and two regulated deficit irrigation (RDI) treatments, in which water application was reduced to 37% (RDI1) and 50% (RDI2) during a deficit irrigation period in the summer (dates are shown in Table 1). Concurrently with the airborne flights over the study site at different crop development stages, a series of leaf measurements were performed (Table 1). Assimilation rate (A; $\mu mol/m^2/s$) and stomatal conductance (Gs, $mmol/m^2/s$) were measured by means of a photosynthesis measurement system (LCDpro-SD: ADC Bioscientific Ltd., Herts, U.K.) on two leaves per tree

Table 1
Flight dates, irrigation doses and field measurements during the 2012 and 2013 airborne and field campaigns.

Year	Treatments	RDI period	Irrigation dose[a]	Flight dates	Type of flight[b]	Field measurements
2012	ET (control)		100%	14/06	Noon (T)	A, Gs, SpectraPen
	RDI1	12/06 to 13/09	37%	26/07	Noon (T + H)	A, Gs
	RDI2	12/06 to 13/09	50%	02/08	Diurnal (T + H)	A, Gs, Ψ, Leaf F (*diurnal trend*)
				04/09	Diurnal (T + H)	A, Gs, Leaf F (*diurnal trend*)
2013	ET (control)		100%	04/06	Noon (T + H)	A, Gs, Leaf F, SpectraPen
	RDI1	18/06 to 12/09	37%	02/07	Noon (T + H)	A, Gs, Leaf F, SpectraPen
	RDI2	18/06 to 12/09	50%	23/08	Noon (T + H)	A, Gs, Ψ, Leaf F
				11/09	Noon (T + H)	A, Gs, Ψ, Leaf F, SpectraPen
				30/10	Noon (T + H)	A, Gs, Leaf F, SpectraPen

[a] % of calculated ETc. Out of the RDI period, 100%ET was applied to every treatment.
[b] T = thermal; H = hyperspectral

on two to four trees in each of the control and RDI treatments. On specific dates, stem water potential (Ψ) was measured on the same trees with a pressure chamber (Model 3005: Soil Moisture Equipment Co., Santa Barbara, CA, USA). Steady-state leaf fluorescence yield (F) and leaf reflectance were measured on ten leaves per tree using FluorPen FP100 and PolyPen RP 400 UVIS instruments, respectively (Photon Systems Instruments, Brno, Czech Republic). These instruments are self-calibrated at the beginning of each session of measurements. The field measurements were carried out concurrently with the airborne measurements, either at midday (12:00 to 13:00 h local time) or following a diurnal trend at intervals between 9:00 h and 13:00 h. Although the leaf fluorescence measurements carried with the FluorPen FP100 were of different nature than the airborne SIF retrievals, the leaf data served as a field-level assessment of the stress for each treatment. The normalized canopy temperature (Tc) to air temperature was calculated using a weather station (Model WXT510, Vaisala Oyj, Helsinki, Finland) installed 1 m above the canopy, which measured air temperature (Ta) and relative humidity (RH).

2.1.2. Airborne campaigns

The airborne campaigns were carried out in 2012 and 2013 flying with the heading of the aircraft on the solar plane, using a thermal camera and a micro-hyperspectral imager installed in tandem on a Cessna aircraft operated by the Laboratory for Research Methods in Quantitative Remote Sensing (QuantaLab), Consejo Superior de Investigaciones Científicas (IAS-CSIC, Spain).

The linear-array hyperspectral camera used in this study was the micro-hyperspec VNIR model (Headwall Photonics, Fitchburg, MA, USA) operated with a configuration of 260 spectral bands acquired at 1.85 nm/pixel and 12-bit radiometric resolution in the 400–885 nm region, and yielding a 6.4 nm FWHM with a 25-μm slit. The acquisition and storage module achieved a 50 fps frame rate with integration time set to 18 ms. The 8 mm focal length lens provided an IFOV of 0.93 mrad and an angular field of view (FOV) of 50°, providing a swath of 380 m at 40 cm pixel resolution at 420 m AGL altitude and 140 km/h ground speed. The micro-hyperspectral sensor was radiometrically calibrated in the laboratory with the CSTM-USS-2000C integrating sphere (LabSphere, North Sutton, NH, USA) at four levels of illumination and six integration times. The hyperspectral imagery was orthorectified using PARGE remote-sensing software (ReSe Applications Schläpfer, Wil, Switzerland), which employed input data acquired with a GPS-enhanced miniature Attitude and Heading Reference System (AHRS) model IG-500n (SBG Systems, Rueil-Malmaison, France) installed on board and synchronized with the micro-hyperspectral imager (Fig. 1).

The thermal imagery was acquired in the 7.5–13 μm range by a FLIR SC655 thermal camera (FLIR Systems, Wilsonville, OR, USA) installed in tandem with the hyperspectral camera on the same aircraft. The camera yields a resolution of 640 × 480 pixels with a 13.1 mm optics focal length, providing an angular FOV of 45° and a ground resolution of 50 cm. The camera's radiometric calibration was performed in the laboratory using a blackbody (model P80P, Land Instruments, Dronfield, UK) and vicarious calibration was performed for each flight using field-measured targets with a thermal gun model LS LT (Optris GmbH, Berlin, Germany). After each flight, thermal images were processed in the laboratory and mosaicked to generate the entire scene (Fig. 2).

A total of four flights in 2012 and five in 2013 were carried out, both at midday and following diurnal trends (Table 1). Two of the nine flights corresponded with diurnal experiments carried in 2012 using both thermal and hyperspectral cameras. Unfortunately, only the thermal imagery was acquired in one of the 2012 midday flights due to failure of the hyperspectral camera (see Table 1 for specific details of the type

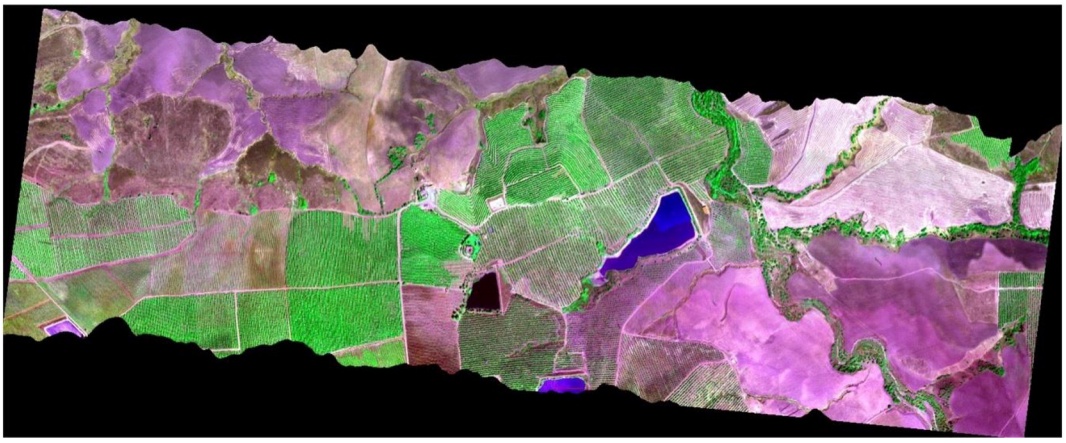

Fig. 1. Hyperspectral mosaic of the entire orchard area flown in the 2012 and 2013 airborne campaigns, with a configuration of 260 spectral bands, 1.85 nm/pixel and 12-bit radiometric resolution in the 400–885 nm region, yielding 40 cm pixel resolution at 420 m altitude. Spectral bands shown are 550 nm (blue), 670 nm (red) and 800 nm (green). (For interpretation of the references to color in this figure legend, the reader is referred to the web version of this article.)

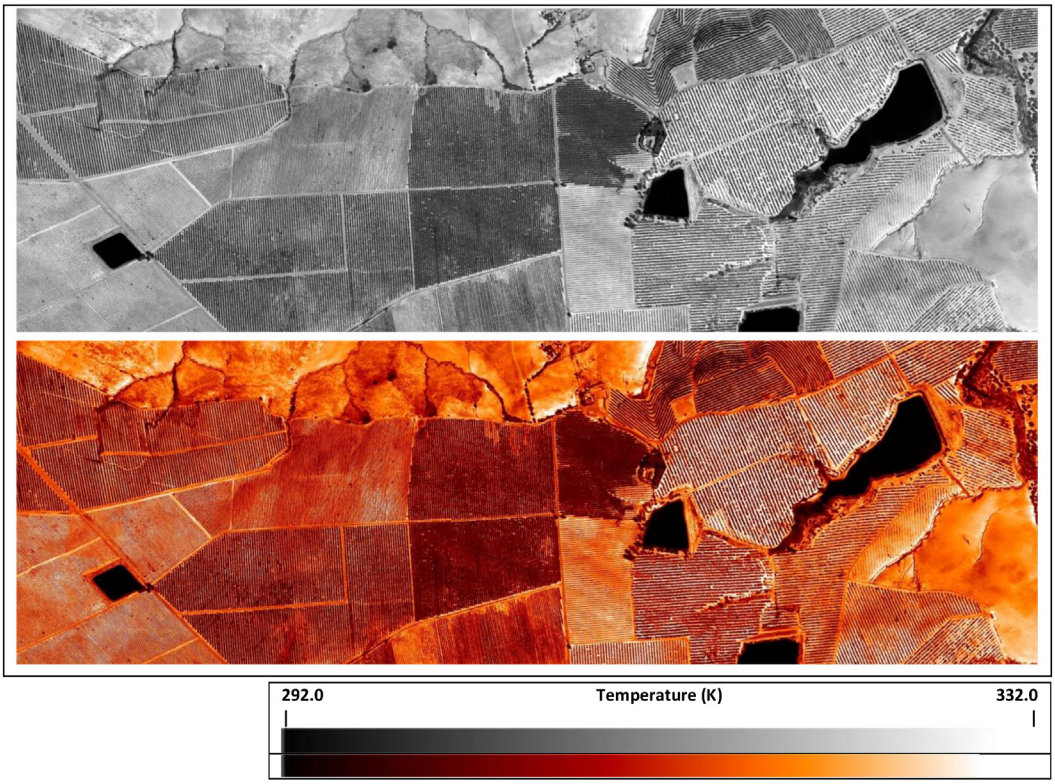

Fig. 2. Thermal mosaic of the orchard area flown in 2012 and 2013 airborne campaigns acquired in the range of 7.5–13 μm with a thermal camera that yielded an angular FOV of 45° and a ground resolution of 50 cm. The upper part shows the thermal image in greyscale, the lower shows the thermal image using a color table to emphasize the spatial variability.

of flights conducted, flight times and dates). The flights took place at the start of the experiment before stress levels were applied, at the time of maximum stress, and after the recovery started following the start of the rewatering scheme. The high-resolution imagery acquired with both thermal and hyperspectral cameras enabled the pure crowns over the entire scene to be identified (Fig. 3), thus enabling shaded and sunlit soil and crown components to be discriminated. Only the sunlit crown components extracted from the imagery were used for the calculation of hyperspectral indices and the fluorescence quantification described in the following section.

2.2. Fluorescence retrieval and hyperspectral indices calculated from the airborne imagery

Additional data were acquired in the field concurrently with each flight in order to obtain surface reflectance for calculating the hyperspectral indices, and quantifying chlorophyll fluorescence using radiance spectra. The atmospheric correction used SMARTS (Gueymard, 1995, 2001, 2002, 2005) with aerosol optical depth measured at 550 nm with a Micro-Tops II sunphotometer (Solar LIGHT Co., Philadelphia, PA, USA). This model has been used in previous studies for both narrow-band multispectral and hyperspectral imagery (Berni, Zarco-Tejada, Suárez, & Fereres, 2009; Zarco-Tejada et al., 2012; Calderon et al., 2013, 2015).

The mean reflectance spectra calculated for the 260 spectral bands acquired by the hyperspectral imager were then used to calculate several spectral indices related to: i) tree crown structure, caused by the sensitivity of the near-infrared bands to the foliar scattering of the canopy (NDVI, RDVI and the normalized family of indices MTVI1, MSAVI, among other indices); ii) epoxidation state of the xanthophyll cycle caused the absorption of three carotenoid pigments that are active in the xanthophyll cycle: violaxanthin (V), antheraxanthin (A), and zeaxanthin (Z) (family of PRI and normalized PRI indices, CAR index); iii) chlorophyll a + b, caused by the absorption of spectral bands in the green, red, and red edge ranges to chlorophyll concentration (including the TCARI, Vogelmann, Carter, and Lichtenthaler family of indices); iv) blue/green/red ratio indices, such as G, BGI1, BGI2); v) chlorophyll fluorescence emission by photosystems I (PS-I) and II (PS-II) (CUR index), and vi) spectral disease index developed for disease detection purposes (HI index) (see Zarco-Tejada et al., 2005, 2012 and Calderon et al., 2013, 2015 for further review of the hyperspectral indices used in this study).

Chlorophyll fluorescence from radiance spectra (Fig. 4a) was quantified using the FLD principle (Plascyk, 1975) as described in Zarco-Tejada et al. (2013c), measuring total incoming irradiance at the time of the flights using a 0.065 nm full-width half-maximum (FWHM) Ocean Optics HR2000 fiber-optics spectrometer (Ocean Optics, Dunedin, FL, USA) with a CC-3 VIS-NIR cosine corrector-diffuser (Ocean Optics). The instrument was housed in a Peltier thermally insulated box (PT-100, Magapor, Zaragoza, Spain) in order to keep the internal temperature stable at 24 °C ± 1 °C during field measurements. Irradiance (E) calibration of the spectrometer attached to the fiber with the cosine corrector-diffuser was performed in the laboratory using a LS-1-CAL calibrated tungsten halogen NIST-traceable light source (Ocean Optics). To match the spectral resolution of the radiance imagery acquired by the hyperspectral airborne sensor, the high-resolution irradiance spectra measured with the HR2000 instrument was resampled through Gaussian convolution. The FLD principle was applied to the hyperspectral imagery to quantify the fluorescence signal using three bands in the O_2-A region (FLD3), considering L_{in} (L_{763}), L_{out} (average of L_{750} and L_{780} bands) from airborne radiance, E_{in} (E_{763}), and E_{out} (average of E_{750} and E_{780} bands) from irradiance spectra (Fig. 4b).

Although the quantification of chlorophyll fluorescence from hyperspectral imagery is at the focus of a current debate, and very-high-resolution spectral data have been proposed for the accurate retrieval of fluorescence in absolute terms, several studies have demonstrated that fluorescence can be retrieved from broader-band low-altitude imaging sensors in terms of relative means and for precision

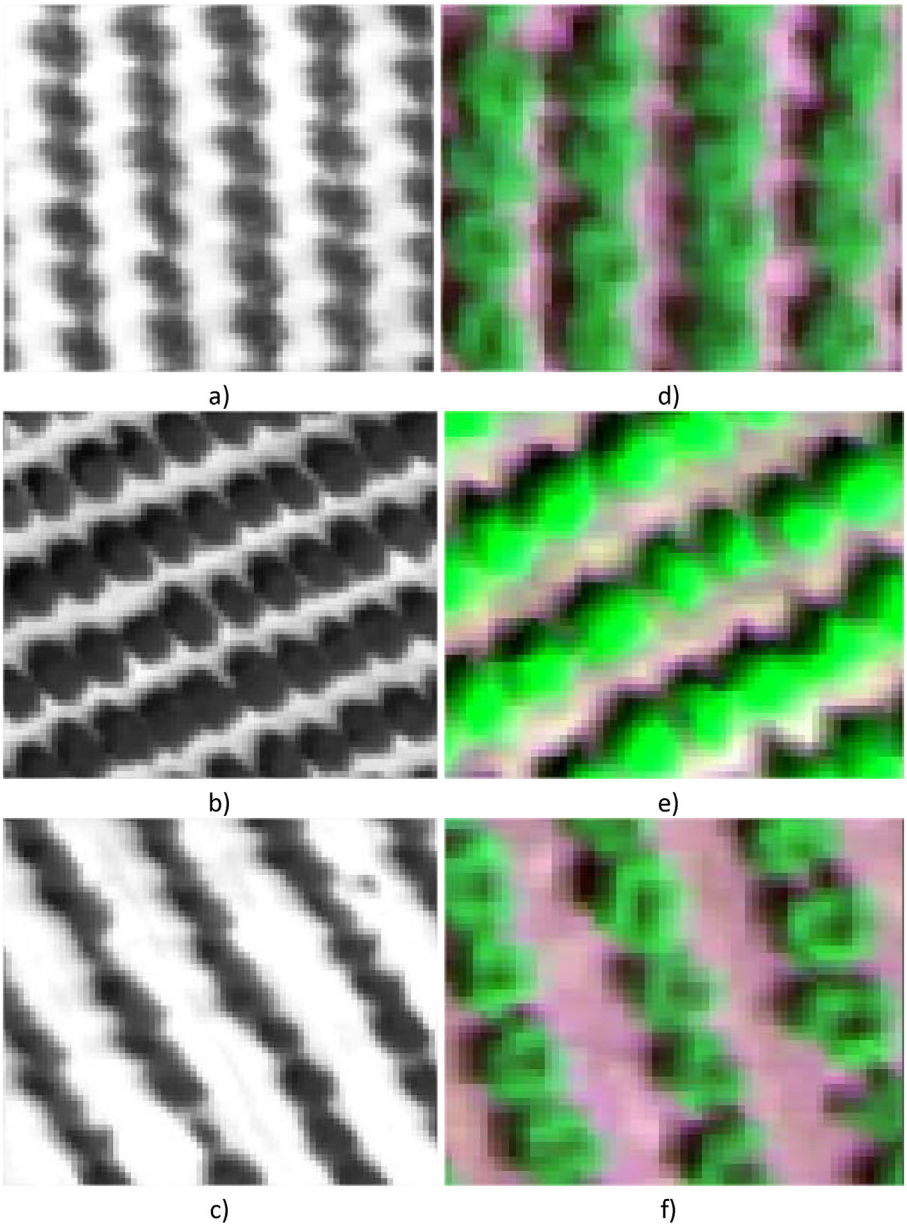

Fig. 3. Sample thermal (a; b; c) and hyperspectral (d; e; f) imagery acquired during the 2012 and 2013 airborne campaigns that enabled the separation of scene components. The sunlit crown components extracted from the imagery were used to calculate hyperspectral indices and quantify fluorescence.

agriculture and stress-detection purposes (Zarco-Tejada et al., 2012, 2013d; Calderon et al., 2013, 2015; Damm et al., 2015). The FLD3 and other approaches to fluorescence quantification as a function of the number of bands, spectral bandwidth, and signal-to-noise ratio of the instrument were reviewed by Meroni et al. (2010), with modelling by Damm et al. (2011) showing that the FLD3 method can retrieve the fluorescence signal when wider spectral bandwidths (e.g. 5 nm FWHM) and high-spectral sampling (below 2.5 nm) with instruments with a minimum of 300:1 signal-to-noise ratio are employed. The methodology used in this experiment, as well as those used by Zarco-Tejada et al. (2012, 2013d) and Calderon et al. (2013, 2015) are therefore suitable for the retrieval of relative fluorescence in the context of stress detection, as the sensor is characterized by 260 bands acquired at 6.4 nm FWHM, 1.85 nm sampling interval (yielding a total of 13 spectral bands inside the O_2-A feature) and a signal-to-noise ratio of 300:1 without spatial binning. A recent study by Damm et al. (2015) supports this methodological approach using APEX airborne imagery with a spectral sampling interval of 4.5 nm and a FWHM of 5.7 nm.

The airborne fluorescence quantification performed for each single crown under different levels of water stress and for each flight date was compared with ground measurements of leaf-level fluorescence and net photosynthesis acquired over the two-year period. In particular, the robustness and stability of the relationships were assessed for each flight date using both the fluorescence quantification and the hyperspectral indices calculated from the reflectance imagery in order to determine whether the fluorescence retrievals and the indices were sensitive to the assimilation levels resulting from the different stress stages and ambient conditions. A normalization method for all fluorescence quantities retrieved from each RDI tree (stressed trees) to the ET treatment as a baseline (non-stressed trees) in the form $FLD_n = FLD_{tree} - FLD_{ET}$ was applied to all trees and dates in this experiment in order to evaluate the seasonal stability of the single F vs A relationship in the context of stress detection and precision agriculture.

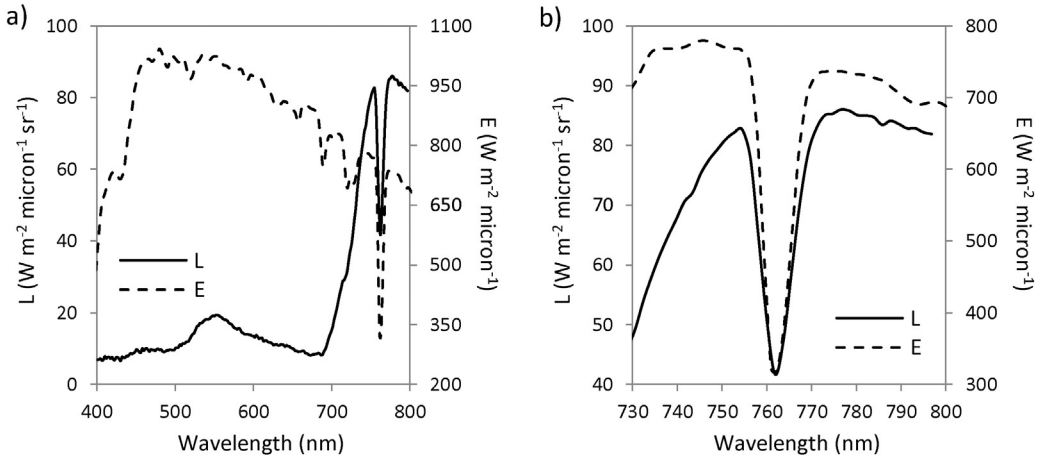

Fig. 4. Pure-vegetation tree crown radiance spectra obtained from the airborne micro-hyperspec VNIR in the 400–800 nm region (a) and in the 730–800 nm region (b). Measured irradiance spectra (a; b) were used to quantify chlorophyll fluorescence and to calculate reflectance indices.

3. Results

The physiological measurements made during the two seasons revealed no differences among treatments at the start of the experiment on stomatal conductance and leaf assimilation (Fig. 5a, b). After the differential irrigation treatments started (indicated with an arrow in Fig. 5), the results of the three treatments began to diverge, reaching maximum differences at the time of maximum stress

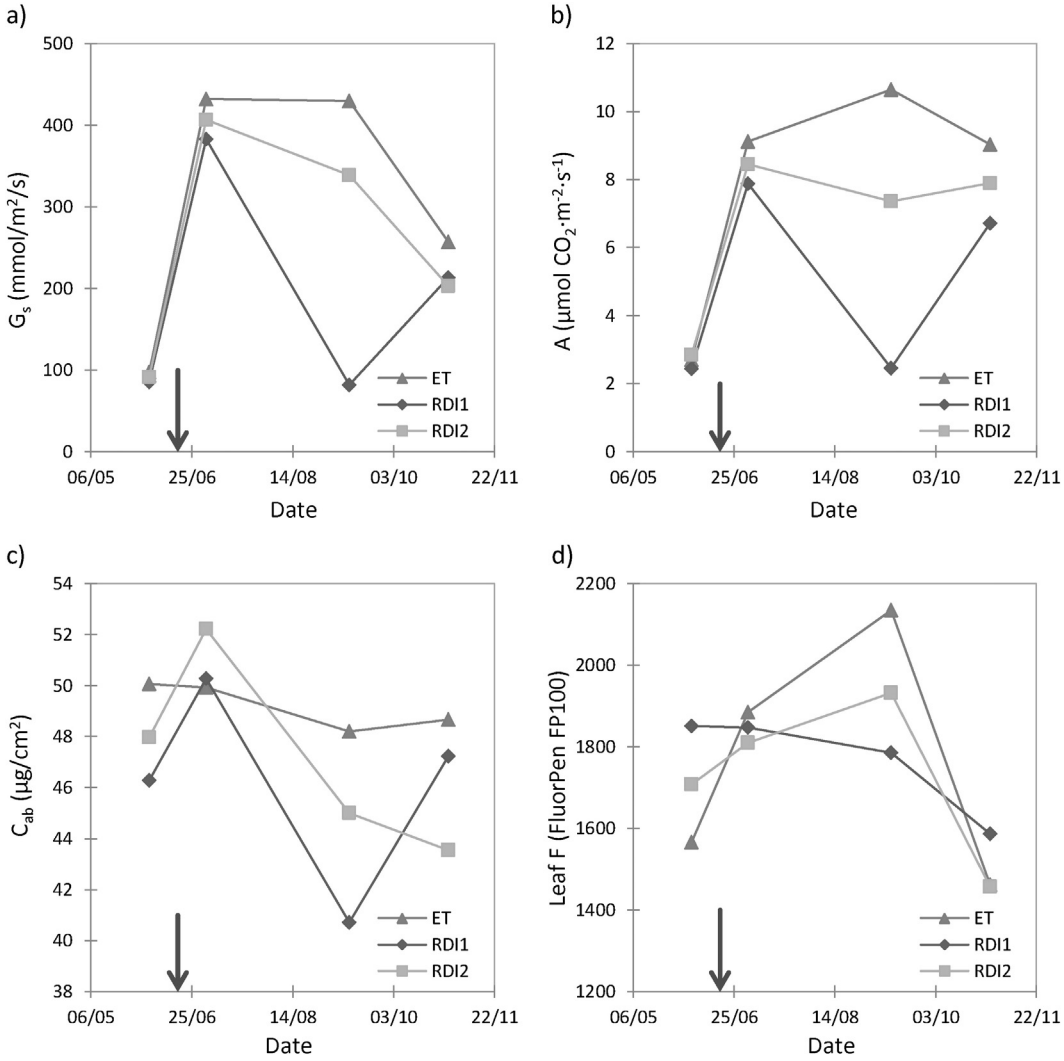

Fig. 5. Leaf-level measurements from the 2013 experiment for stomatal conductance, Gs (a), assimilation, A (b), chlorophyll content (c) and leaf fluorescence (F) measured with the FluorPen FP100 (d). The arrows indicate the beginning of the water-stress experiment.

($\Psi = -1.94$ MPa for RDI1; $\Psi = -1.06$ MPa for ET) (Table 2). The values obtained for Gs and A showed large treatment differences on the date of maximum stress (Sept. 11th), reaching 429.9 mmol/m^2/s and 10.65 μmol CO_2/m^2/s (ET) compared to 81.9 mmol/m^2/s and 2.4 μmol CO_2/m^2/s (RDI1). After rewatering on September 12th, both Gs and A rates converged to values around 200–250 mmol/m^2/s and 6.7–9 μmol CO_2/m^2/s. Chlorophyll content (Cab) calculated from the leaf reflectance measurements was stable for the ET treatment over the course of the experiment (Fig. 5c), while the RDI treatments decreased at the time of the maximum stress ($C_{ab} = 40.7$ μg/cm^2 for RDI; $C_{ab} = 48.2$ μg/cm^2 for ET).

Nevertheless, the differences observed in Cab at the beginning of the experiment (ranging from 46 to 50 μg/cm^2 among treatments) were also detected, but inversely related, in the leaf-level fluorescence (F) measurements (Fig. 5d). The leaf F data showed lower values for the ET treatment than for the RDI1 treatment before the stresses were applied ($F_{RDI1} > F_{RDI2} > F_{ET}$), but displayed the opposite behavior at the time of maximum stress ($F_{ET} > F_{RDI2} > F_{RDI1}$). At the end of the experiment (after rewatering), the F values converged, showing the same levels for F_{RDI2} and F_{ET}. These leaf-level physiological measurements measured with the FluorPen FP100 instrument demonstrated that the irrigation treatments created a gradient in tree water status, with wide differences in stress levels needed for the assessment of the fluorescence quantification from the airborne imagery, starting with similar physiological conditions at the beginning of the experiment, following a period of maximum stress, and a recovery after rewatering began. The results of the leaf spectral measurements showed seasonal variations in the reflectance spectra collected from the ET (Fig. 6a) and RDI (Fig. 6b) treatments. An increase in leaf reflectance at the red and red-edge regions, associated with a decrease in chlorophyll content as the trees were moving into stress, is noticeable for both ET and RDI treatments.

A close look at the visible region shows the spectral differences related to chlorophyll absorption at the beginning of the experiment (Fig. 7a), their increase, and the time of maximum stress levels (Fig. 7b), disappearing at the end of the experiment (Fig. 7c).

These results show that the leaf spectral measurements were also sensitive to the stress levels imposed, tracking the physiological changes forced by the irrigation experiment. The diurnal experiments performed on two dates in 2012 showed consistent patterns of assimilation rate (Fig. 8a), stomatal conductance (Fig. 8b) and fluorescence (Fig. 8c), measured at leaf level; maximum values were recorded early in the morning and showed a gradual decrease until midday. Differences between treatments (ET and RDI1) were also at a maximum during the first hours of the day, although both treatments reached values close to 0 for Gs and A at midday. The diurnal course of stomatal closure induced by low VPD in citrus under well-watered conditions has been already observed (Villalobos, Testi, & Moreno-Perez, 2009; Roccuzzo, Villalobos, Testi, & Fereres, 2014), and our results are consistent with previous experiments. The relationships obtained between A and Gs (Fig. 9a) and between A and F (Fig. 9b) yielded statistically significant results ($r^2 = 0.66$), confirming for this experiment that leaf

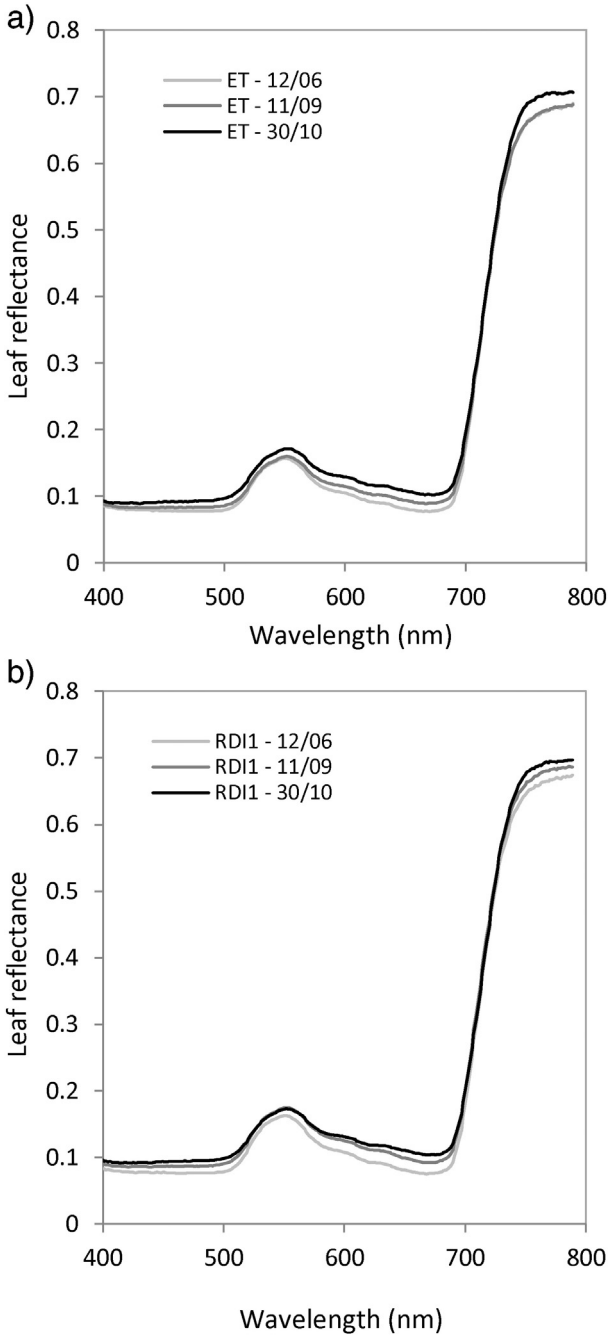

Fig. 6. Leaf spectra acquired at the beginning (12/06), maximum stress (11/09) and end stages of the experiment (30/10) for ET (well-watered) (a) and RDI (water-stressed) (b) leaves.

Table 2
Water potential, stomatal conductance and assimilation data measured during the 2012 and 2013 airborne and field campaigns.

Year	Dates	A (μmol/m^2/s)			Gs (mmol/m^2/s)			Ψ (MPa)		
		ET	RDI1	RDI2	ET	RDI1	RDI2	ET	RDI1	RDI2
2012	14/06	1.29	0.86	–	54.6	51.0	–	–	–	–
	26/07	15.89	5.88	12.70	–	–	–	−0.92	−2.02	−1.11
	02/08	1.09	0.62	–	182.8	57.8	–	−0.89	−2.53	–
	04/09	3.77	0.98	–	114.5	17.3	–	–	–	–
2013	04/06	2.70	2.43	2.85	97.3	85.4	91.3	–	–	–
	02/07	9.12	7.89	8.45	432.2	382.9	406.9	–	–	–
	23/08	6.10	2.09	5.27	633.1	128.6	177.7	−1.06	−1.94	−1.03
	11/09	10.65	2.45	7.36	430.0	81.9	338.6	−0.86	−1.65	−0.96
	30/10	9.03	6.71	7.90	257.0	213.4	202.9	–	–	–

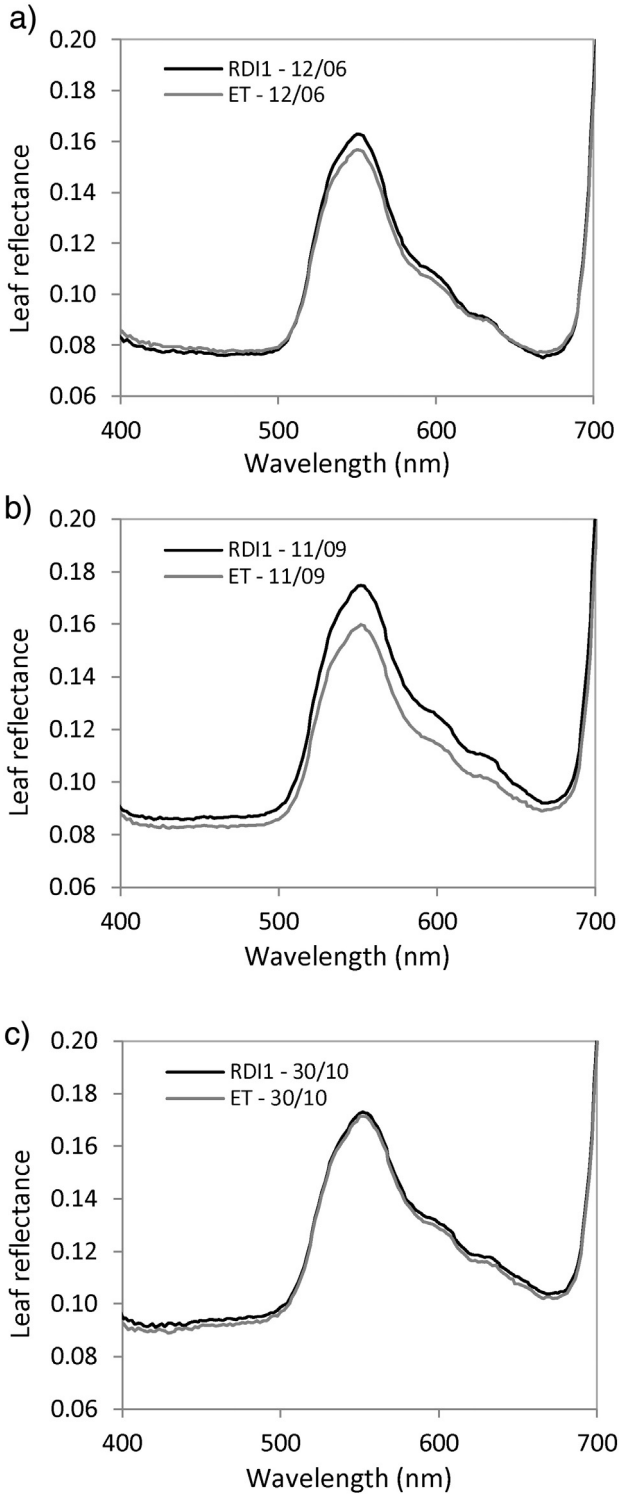

Fig. 7. Leaf spectra measured in the 400–700 nm region on three dates during the experiment for RDI (water-stressed) and ET (well-irrigated), showing the small differences related to chlorophyll at the beginning of the experiment, 12/06 (a) that increased at the time of maximum stress, 11/09 (b), disappearing after rewatering, 30/10 (c).

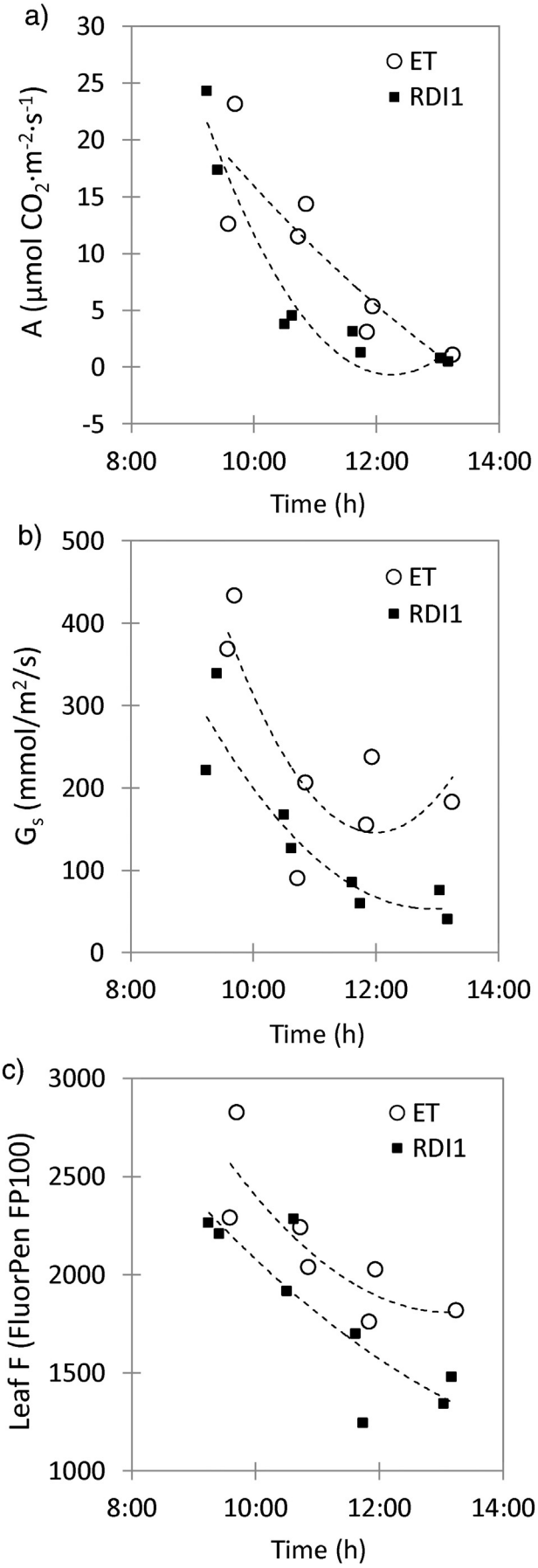

fluorescence closely tracked the diurnal changes in assimilation. In fact, A–F yielded a more robust relationship than the well-known A–Gs (see Flexas, Bota, Escalona, Sampol, & Medrano, 2002 for A–Gs and A–F relationships). At the time of the maximum stress (September 4th) differences in stomatal conductance (Fig. 10a) and assimilation rate (Fig. 10b) between the two treatments were at their maximum,

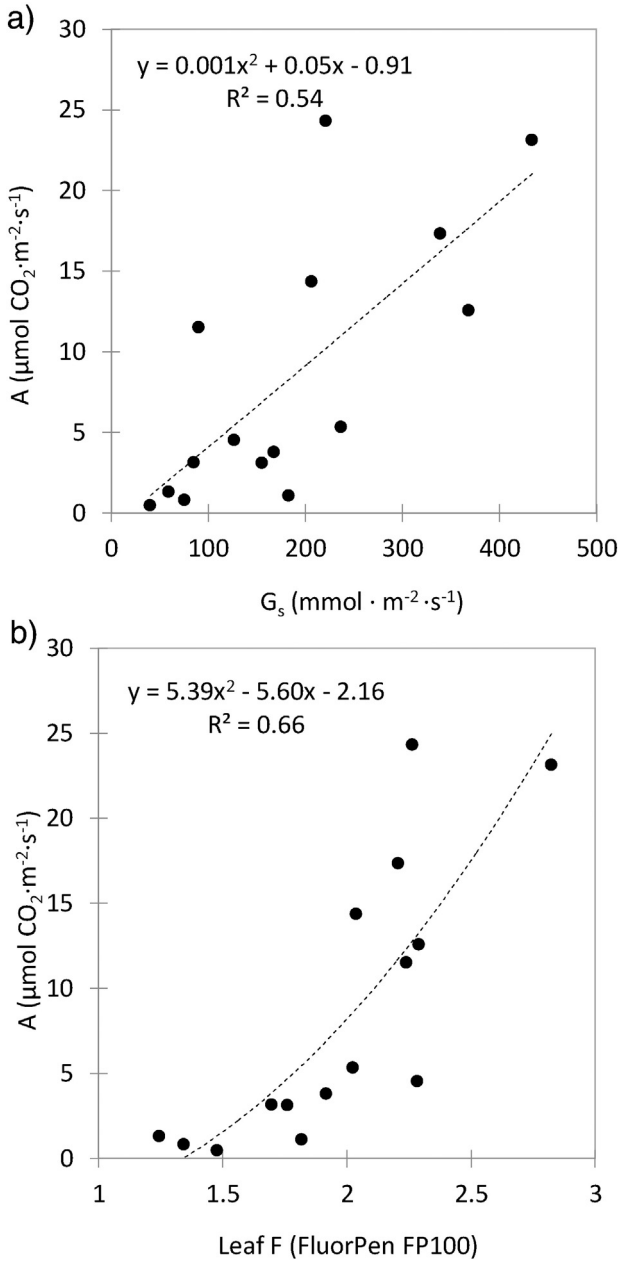

Fig. 9. Leaf-level relationships from the diurnal study performed on August 2nd, 2012, between assimilation, A vs stomatal conductance, Gs (a), and fluorescence (FluorPen readings) (b).

especially at midday. Daily trends were similar to those observed in Fig. 8, although values for control trees at midday were higher than in August. These differences were related to a milder evaporative demand in September (VPD = 3.1 kPa) than in August (VPD = 4.4 kPa). Similar results have been observed in other experiments in olive trees (Moriana, Villalobos, & Fereres, 2002), confirming the consistency of the data obtained here. The relationship between airborne fluorescence (FLD) and A for the ET and RDI1 treatments measured at the two flight times (morning; midday) showed a consistent trend (Fig. 10c) that depicts the diurnal tracking of A by airborne fluorescence.

The results of the relationships obtained between assimilation (A) and thermal and hyperspectral indices calculated for each date are

Fig. 8. Leaf-level measurements from the diurnal study on August 2nd, 2012 for assimilation (A) (a), stomatal conductance (Gs) (b), and leaf fluorescence (F) measured with the FluorPen FP100 (c).

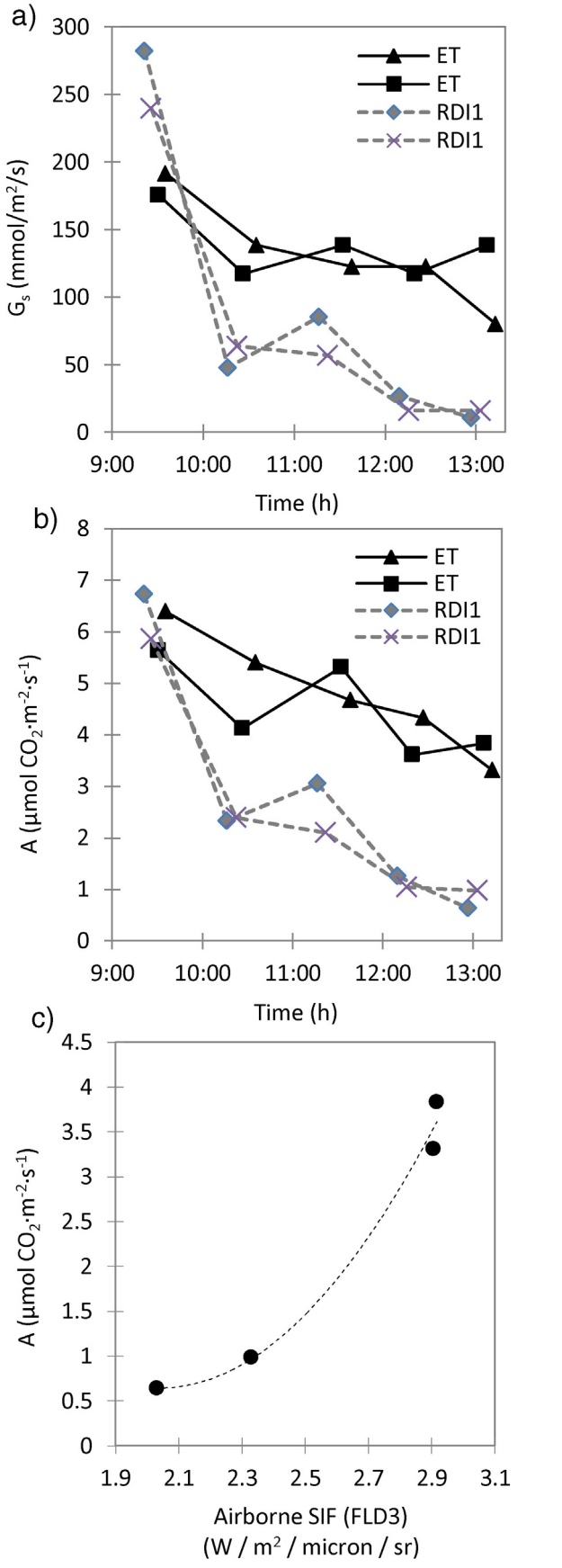

Fig. 10. Results of the diurnal study performed on September 4th, 2012, showing stomatal conductance, Gs (a) and assimilation, A (b) for two trees under RDI1 (water-stressed) and ET (well-irrigated) treatments, and the trend between airborne SIF (FLD3) and assimilation, A, for the ET and RDI1 treatments measured at two flight times (c).

Table 3
p-Values obtained for the relationships between A and all indices on each date. Shaded areas indicate the different levels of significance.

Index	26–07–12	04–06–13	02–07–13	23–08–13	11–09–13	30–10–13
Thermal						
Tc–Ta	0.1050	0.5569	0.0303	0.1563	0.0008	0.5518
Fluorescence						
SIF (FLD3)	0.0002	0.0050	0.0001	0.0000	0.0021	0.0003
CUR	0.0024	0.7885	0.0174	0.0957	0.0191	0.1794
Photosynthetic pigments						
CI	0.1612	0.0002	0.2086	0.9631	0.2505	0.2540
TCARI	0.0023	0.3075	0.4096	0.0940	0.0068	0.1452
TCARI/OSAVI	0.0498	0.0744	0.4433	0.1033	0.0109	0.1703
TVI	0.0002	0.0128	0.0606	0.0255	0.0177	0.0656
VOG	0.0987	0.0052	0.1562	0.7062	0.1064	0.2401
VOG2	0.1700	0.0003	0.1703	0.5612	0.1734	0.2300
VOG3	0.1799	0.0004	0.1727	0.6115	0.1728	0.2420
SRPI	0.0678	0.5047	0.3394	0.2501	0.2206	0.0503
NPQI	0.2268	0.7201	0.6694	0.7571	0.0353	0.0013
NPCI	0.0639	0.5030	0.3401	0.2785	0.2087	0.0497
CTR1	0.3044	0.5930	0.3170	0.3558	0.1208	0.0089
LIC1	0.0521	0.0009	0.2853	0.2227	0.4149	0.2724
LIC2	0.1292	0.0599	0.2991	0.2610	0.1794	0.0411
LIC3	0.0461	0.0053	0.4508	0.3144	0.1909	0.3025
SIPI	0.0597	0.0001	0.3085	0.1652	0.5399	0.2806
CAR	0.0311	0.1362	0.6180	0.1530	0.0481	0.6856
PRI	0.3456	0.7208	0.1652	0.1121	0.0141	0.1154
PRIM1	0.0084	0.0299	0.6793	0.0563	0.0181	0.5020
PRIM2	0.0148	0.0007	0.4493	0.1285	0.0519	0.2089
PRIM3	0.0059	0.0062	0.4075	0.0753	0.0800	0.3219
PRIM4	0.0063	0.0259	0.4001	0.0947	0.0362	0.5179
PRIn	0.0678	0.0639	0.2791	0.2243	0.0020	0.2379
PRI_{515}	0.0107	0.0330	0.5810	0.0803	0.0215	0.4808
BGI1	0.0581	0.6461	0.0753	0.2356	0.0016	0.1169
BGI2	0.0004	0.2156	0.4430	0.0459	0.0590	0.1446
G	0.0033	0.0033	0.3932	0.0663	0.0576	0.3226
HI	0.0330	0.0182	0.1943	0.0285	0.1652	0.1556
Structural						
NDVI	0.0608	0.0004	0.3073	0.2278	0.4632	0.3096
RDVI	0.0034	0.0013	0.0306	0.0002	0.0173	0.0672
SR	0.0628	0.0002	0.3265	0.1783	0.6636	0.1930
MSR	0.0619	0.0003	0.3250	0.1922	0.6129	0.2230
EVI	0.0060	0.0013	0.0510	0.0001	0.0382	0.1249
MTVI1	0.0007	0.0039	0.0371	0.0024	0.0077	0.0260
MSAVI	0.0048	0.0014	0.0524	0.0002	0.0249	0.0830
MCARI1	0.0023	0.0003	0.0860	0.0009	0.0182	0.2066

n.s. | $p<0.05$ | $p<0.01$ | $p<0.001$ | $p<0.0001$

shown in Table 3. The *p*-values shown in the table point out the indicators that are sensitive across all dates, comprising the thermal, fluorescence, photosynthetic pigments and structural indices. The table also shows that the indicators showing the highest sensitivity against A across all flight dates were fluorescence (FLD3) and the structural indices RDVI and MTVI1, these three being the only indicators that were statistically significant ($p < 0.05$) on all dates or all dates except one. The relationships obtained for fluorescence (FLD3), structural index RDVI, and chlorophyll index TCARI against A for each single date can be seen in Fig. 11, using second-order polynomials. As the figure shows, the variability of the relationships across dates is higher for RDVI and TCARI, with some dates not being statistically significant (Table 3), given their low coefficients of determination (Fig. 11). The relationships between fluorescence (FLD3) and assimilation yielded correlation coefficients (R) between 0.64 and 0.82 across all dates, all of which were statistically significant (Table 4), with *p*-values between <0.05 and <0.0001 (Table 5). Although the structural index MTVI1 was also statistically significant on all dates (Table 3), the correlation coefficients (Table 4) showed poorer performance than FLD3, and the statistical significance was also lower (Table 5). This assessment was performed on groups of functional indicators in order to determine whether the linear combination of functional types would explain assimilation rates (A) with higher statistical significance. Fluorescence (FLD3), the structural indices MTVI1 and RDVI, and chlorophyll indices TCARI, TVI, CI were linearly combined, showing the sensitivity to assimilation A on all dates. The results shown in Tables 4 and 5 suggest that fluorescence combined with structural or chlorophyll indicators would only marginally improve the sensitivity to A.

The stability of the fluorescence (SIF FLD3) vs assimilation (A) relationships, assessed seasonally across all dates, showed that they did not correspond to a single relationship (Fig. 12a).

This is probably due to the nature of the relationship itself (fluorescence used as a proxy for assimilation rates), but also to the inherent offsets of the FLD approach created when calculated from broader bandwidth imagery (i.e., 5–6 nm FWHM) that would generate variable absolute errors, which will be a function of the irradiance levels measured at the O_2-A band with such spectral resolution. An approach based on normalization of the FLD3 value from each tree to the fully irrigated (non-stressed) fluorescence value for each date was adopted, giving a single relationship of FLD3 vs A for the entire season using all flight dates ($r^2 = 0.5$; $p < 0.0001$; Fig. 12b). These normalized fluorescence values obtained over the entire season showed better results compared to assimilation (A) than to NDVI ($r^2 = 0.01$; n.s.; Fig. 12c) and MTVI1 ($r^2 = 0.27$; $p < 0.0001$; Fig. 12d) structural indices (the normalization approach applied to structural indices did not yield good results; data not shown). The normalization approach taken here for FLD3 has previously been proposed for thermal imagery and water-stress detection studies, using the well-watered trees as the reference for the entire orchard, such as trunk diameter fluctuations (Goldhamer & Fereres, 2001), and might be an appropriate strategy for using the fluorescence signal obtained with broader spectral bands (i.e. above 1 nm FWHM) in the context of precision agriculture. This strategy was scaled up to the treatment level, which enabled us to evaluate the time series for A and for the airborne-quantified FLD3 normalized to the well-irrigated FLD3 ($FLD3_{ET}$) for both the fully irrigated (ET) and stressed (RDI1) blocks for all flights throughout the season (Fig. 13). It can be seen that FLDn tracked A throughout the season from the beginning of the experiment, being sensitive to the larger differences in A at the time of maximum stress. Moreover, it shows that the FLDn trend mimicked the seasonal variation in A at the treatment level, yielding a significant relationship when all treatments (3) and dates (5) were related ($r^2 = 0.72$; $p < 0.0001$; Fig. 14).

4. Discussion

Our results confirm the link between airborne-retrieved fluorescence and assimilation rates during different phenological stages, fluorescence being a more sensitive indicator to photosynthesis than structural, physiological indices and canopy temperature. While canopy temperature showed a strong link with A only at the times of the maximum water-stress levels, the reflectance-based indicators were sensitive to A at specific stages; in all cases they showed less sensitivity to A than chlorophyll fluorescence. Among all the indices, the structural MTVI1 index was related to A on all dates throughout the season, but displayed lower statistical significance and correlation coefficients than airborne quantified FLD fluorescence. As discussed by Zarco-Tejada et al. (2013c), the sensitivity of specific structural and physiological indices to A in the case of evergreen canopies with low phenological dynamics may be due in part to the effects of fluorescence emissions in the 650–850 nm region. Further work using both modelling and experimental data is required to understand the significance of the fluorescence emission signal on structurally sensitive indices (i.e. NDVI, RDVI, MTVI1), chlorophyll indices (such as TCARI), and red-edge ratio indices (such as R_{750}/R_{710}, among others), because the fluorescence emission signal is superimposed on the apparent reflectance, thus affecting such narrow-band indices.

Great progress has been made on the quantification of SIF using sub-nanometer instruments during the past ten years (Meroni et al., 2004, 2008a, 2008b, 2009; Moya et al., 2004; Pérez-Priego et al., 2005), demonstrating the successful retrieval of fluorescence using the O_2-A band

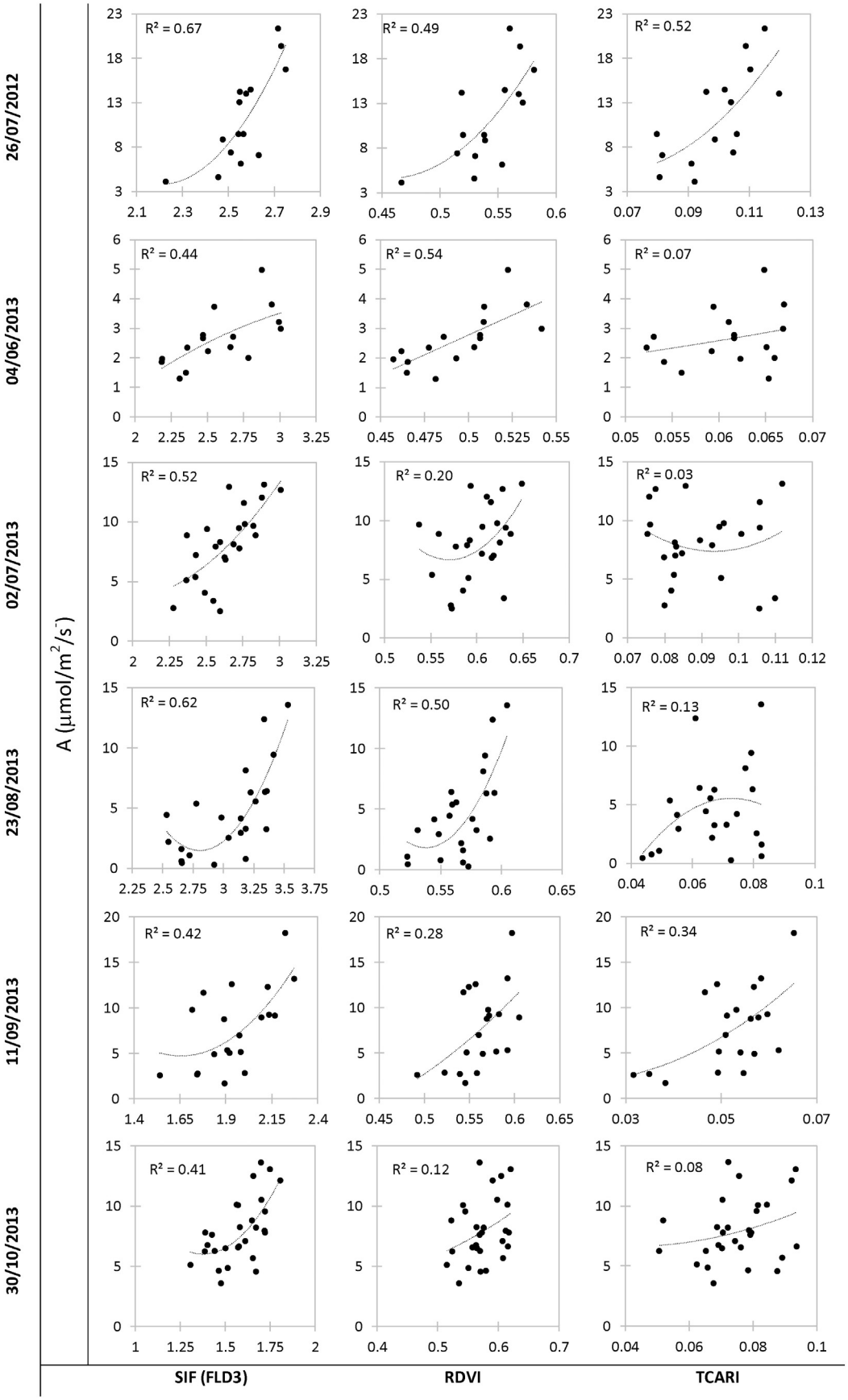

Fig. 11. Relationships for single dates between leaf A and airborne F, RDVI and TCARI using second order polynomial models. SIF (FLD3) units in W/m^2/µm/sr.

Table 4
Correlation coefficient R on all dates between A and selected airborne indices, including combined functional indices.

Functional–related indices	R	26–07–12	04–06–13	02–07–13	23–08–13	11–09–13	30–10–13
Fluorescence	FLD3	0.82	0.66	0.72	0.79	0.65	0.64
Structure	RDVI	0.70	0.73	0.44	0.71	0.53	0.35
	MTVI1	0.78	0.68	0.43	0.60	0.58	0.42
Chlorophyll	TCARI	0.72	0.27	0.17	0.36	0.58	0.28
	TVI	0.81	0.61	0.39	0.46	0.52	0.35
	CI	0.38	0.81	0.27	0.01	0.27	0.22
Structure · Chlorophyll	RDVI · TCARI	0.80	0.52	0.17	0.38	0.60	0.32
	RDVI · TVI	0.79	0.66	0.42	0.55	0.53	0.36
	RDVI · CI	0.47	0.88	0.36	0.49	0.22	0.12
	MTVI1 · TCARI	0.80	0.52	0.14	0.38	0.61	0.35
	MTVI1 · TVI	0.80	0.65	0.41	0.54	0.56	0.39
	MTVI1 · CI	0.61	0.81	0.44	0.72	0.43	0.18
Fluorescence · Structure	FLD3 · RDVI	0.82	0.72	0.68	0.86	0.66	0.58
	FLD3 · MTVI1	0.85	0.70	0.67	0.81	0.67	0.56
Fluorescence · Chlorophyll	FLD3 · TCARI	0.84	0.57	0.35	0.60	0.70	0.45
	FLD3 · TVI	0.88	0.68	0.66	0.76	0.66	0.53
	FLD3 · CI	0.52	0.83	0.58	0.66	0.54	0.30
Fluor · Structure · Chlorophyll	FLD3 · RDVI · TCARI	0.86	0.63	0.39	0.63	0.70	0.45
	FLD3 · RDVI · TVI	0.85	0.70	0.61	0.77	0.65	0.49
	FLD3 · RDVI · CI	0.61	0.82	0.56	0.80	0.57	0.34
	FLD3 · MTVI1 · TCARI	0.85	0.62	0.40	0.62	0.69	0.46
	FLD3 · MTVI1 · TVI	0.85	0.70	0.60	0.74	0.65	0.49
	FLD3 · MTVI1 · CI	0.71	0.78	0.59	0.87	0.58	0.41

Correlation coeff. (R)
0 1

region. The methods and instruments required for the seasonal monitoring of F are now better understood, with recent studies demonstrating operational feasibility of this procedure on seasonal scales (Cogliati et al., 2015). Nevertheless, the transfer of these F-retrieval methods from point-scale to image-scale is more complex and not straightforward. While reasonably priced spectrometers for leaf-level and near-canopy level measurements are widely available (e.g. the high-resolution Ocean Optics instruments), corresponding imaging sensors with sub-nanometer resolution are extremely expensive and not easily available (e.g. HyPlant, among other emerging options). These image-level instruments with sub-nanometer resolutions are therefore not suitable for cost-effective operational applications, even those of great commercial interest such as precision agriculture, stress detection and plant phenotyping. However, the cost and complexity of operating hyperspectral imagers have fallen dramatically in the course of the past 20 years: in the late nineties most hyperspectral work used imagers operated by national institutions such as NASA (AVIRIS) in the USA, DLR in Germany (DAIS/ROSIS), HyMap in Australia and CASI in Canada. Most efforts in remote sensing of vegetation physiology were therefore performed by large research organizations, with little or no studies related to commercial activities or operational vegetation monitoring. Nowadays, the situation is quite different, and new solutions provide the opportunity to successfully operate hyperspectral cameras at lower cost

Table 5
p-Values on all dates between A and selected airborne indices, including combined functional indices.

Functional–related Indices	p–values	26–07–12	04–06–13	02–07–13	23–08–13	11–09–13	30–10–13
Fluorescence	FLD3	0.000202	0.005032	7.25E–05	7.56E–06	0.002072	0.000255
Structure	RDVI	0.003443	0.001253	0.030625	0.00017	0.017255	0.067206
	MTVI1	0.000666	0.003922	0.037068	0.002374	0.007688	0.025989
Chlorophyll	TCARI	0.002322	0.307506	0.409584	0.09395	0.006796	0.145188
	TVI	0.000223	0.012775	0.060603	0.025476	0.017674	0.065623
	CI	0.161186	0.000161	0.208621	0.963111	0.250507	0.253974
Structure · Chlorophyll	RDVI · TCARI	0.000358	0.038854	0.439834	0.075929	0.005349	0.099446
	RDVI · TVI	0.000422	0.005327	0.043287	0.006897	0.016026	0.060689
	RDVI · CI	0.079796	6.76E–06	0.083054	0.017466	0.345688	0.548772
	MTVI1 · TCARI	0.000336	0.036968	0.51221	0.070814	0.00454	0.06686
	MTVI1 · TVI	0.000352	0.006242	0.046404	0.008297	0.010831	0.041971
	MTVI1 · CI	0.016573	0.000138	0.030838	0.000119	0.061503	0.372105
Fluorescence · Structure	FLD3 · RDVI	0.000204	0.001782	0.000268	1.17E–07	0.001407	0.001314
	FLD3 · MTVI1	5.42E–05	0.002374	0.000358	2.7E–06	0.001105	0.001863
Fluorescence · Chlorophyll	FLD3 · TCARI	7.94E–05	0.021083	0.095265	0.002305	0.000535	0.016705
	FLD3 · TVI	1.94E–05	0.003683	0.000463	2.22E–05	0.001444	0.00403
	FLD3 · CI	0.047107	6.59E–05	0.002845	0.000636	0.013032	0.126421
Fluor · Structure · Chlorophyll	FLD3 · RDVI · TCARI	3.91E–05	0.009142	0.060279	0.001242	0.000661	0.016441
	FLD3 · RDVI · TVI	6.62E–05	0.002324	0.001452	1.76E–05	0.00197	0.007637
	FLD3 · RDVI · CI	0.015651	0.000102	0.004464	4.4E–06	0.008936	0.076735
	FLD3 · MTVI1 · TCARI	4.96E–05	0.010142	0.053199	0.001628	0.000775	0.014791
	FLD3 · MTVI1 · TVI	5.79E–05	0.002735	0.002024	6.09E–05	0.0018	0.007959
	FLD3 · MTVI1 · CI	0.00283	0.00034	0.002509	9.69E–08	0.007075	0.028294

n.s. $p<0.05$ $p<0.01$ $p<0.001$ $p<0.0001$

(e.g. sensors such as the micro-hyperspec from Headwall Photonics, Pica from Resonon, among others), with FWHM in the range of 2–10 nm, large sampling intervals and reasonable SNR values. Lightweight hyperspectral cameras, specifically designed for unmanned vehicles (such as the micro- and nano-hyperspectral camera from Headwall Photonics, among others), have become available in recent years, and new frame-based multispectral and hyperspectral cameras are growing rapidly in number (e.g. the hyperspectral cameras from Rikola, UHD 185 from Cubert, Compact Spectral Imager COSI, and OXI cameras from Gamaya, to name only a few). Although the scientific community is currently biased towards global coverage studies for photosynthesis assessment for very important scientific reasons, such as computing the carbon sequestration potential of different plant communities, the global C balance related to climate change studies (e.g. global maps of chlorophyll fluorescence published by Frankenberg et al., 2011 and Joiner et al., 2011, using the Thermal And Near infrared Sensor for carbon Observation (TANSO) on board GOSAT (Kuze, Suto, Nakajima, & Hamazaki, 2009), and using spectra from the Global Ozone Monitoring Experiment-2 (GOME-2) instrument onboard the MetOp-A platform, as described by Joiner et al., 2013 and Guanter et al. 2014), the low spatial resolution of such studies still does not provide a complete understanding of the fluorescence signal when retrieved from mixed pixels that are affected by background, shadows and different amounts of vegetation, all of which need to be correctly interpreted through the use of high-resolution imagery and radiative transfer models (Zarco–Tejada et al., 2013b). Lightweight low-cost hyperspectral systems may serve this purpose, but important specific strategies need to be developed for their correct use for validation purposes and in real applications. With hyperspectral instruments of sub-optimal spectral resolutions for retrieving fluorescence, the atmospheric effects on the algorithms used for chlorophyll fluorescence quantification play a more important role than when sub-nanometer resolutions are available. Furthermore, although the atmospheric effects are smaller when low-altitude airborne platforms (i.e. flying at 300–500 m AGL) are employed, these should not be neglected. A number of studies have recently investigated such impacts of the atmosphere on SIF retrieval (e.g. Daumard, Goulas, Ounis, Pedrós, & Moya, 2015). In fact, this issue is brought to light here in the results of Fig. 12a, which shows a changing relationship between A and SIF as a function of date. A given spectral resolution (in combination with spectral sampling) may cause a specific absolute retrieval error that is approximately constant. In this case, such effects were minimized by the fact that the altitude was constant for all flights and they were performed at the same time under clear-sky conditions typical of the southern European summer. Our interpretation regarding the changing offset and amplitude of the relationships shown in Fig. 12a is twofold: i) as mentioned above, there are potential effects due to slight atmospheric changes, probably due more to changes in the sun angle in the course of the season than actual changes in the optical depth of the atmosphere at different dates; and ii) we believe that the relationship between fluorescence and assimilation is modulated not only by the irradiance levels (i.e. the atmosphere plays an important role) but also by the stress levels at any given time during the season. In summary, in a crop grown under water-limited conditions, the fluorescence vs assimilation relationship varies as a function of the stress level. For this reasons, specific strategies need to be developed for the proper use of chlorophyll fluorescence measurements in agriculture, forestry and plant phenotyping applications. In this study we propose the use of fluorescence normalized by the fluorescence emitted by the unstressed (control, well-watered) trees, which serve as a reference. Although other alternatives exist, e.g. normalizing against non-fluorescence targets, our approach demonstrates the feasibility of using the normalized fluorescence as an indicator of stress levels, both spatially and temporally throughout the season.

Through the adoption of a suitable set of strategies, critical progress has been made in the past 5 years, which has demonstrated that

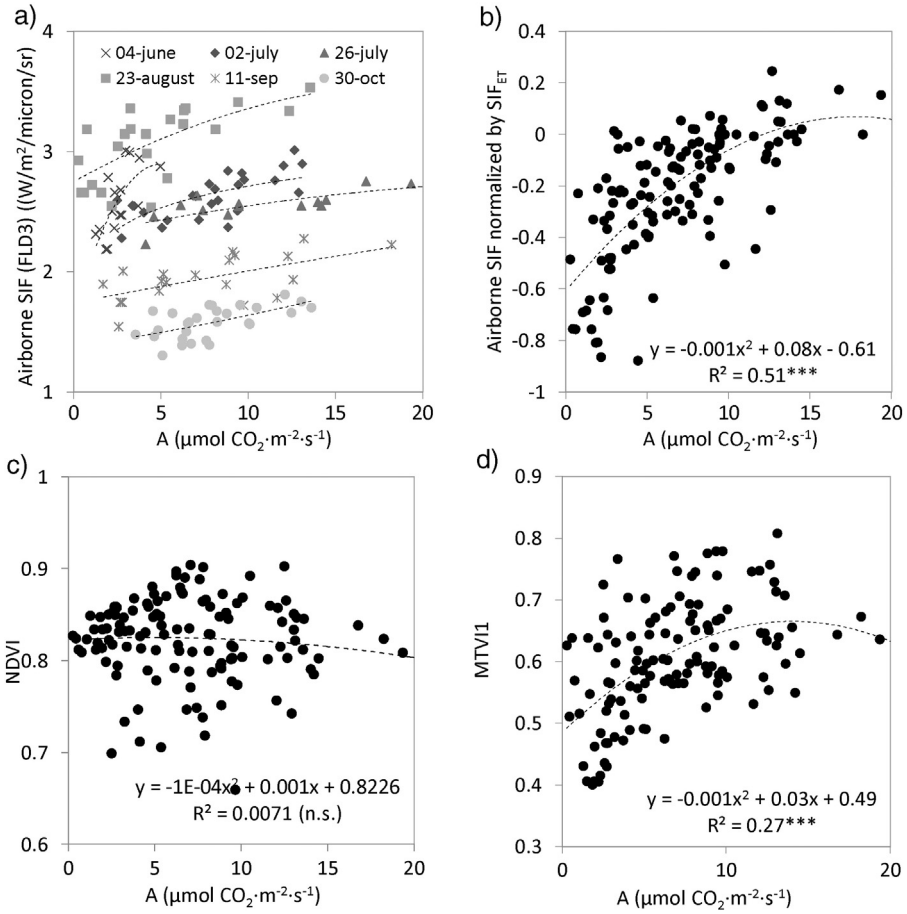

Fig. 12. Relationships between airborne-quantified SIF and leaf assimilation on all single dates of the 2013 campaigns. (a) SIF (FLD3) normalization performed on the airborne-quantified fluorescence retrieved from each tree to the well-irrigated (non-stressed, F_{ET}) value for each date, obtaining a single relationship SIF normalized (F_n) vs A for the entire season using all flight dates. (b) Relationships between structural indicators NDVI (c) and MTVI1 (d) vs A for the entire 2013 campaign.

very high spatial resolution imagery for fluorescence retrievals is essential for the proper validation of simulation models, and for the particular case of stress detection in the context of precision agriculture, precision irrigation, plant phenotyping and precision forestry. An example of potential applications in plant pathology is the early detection of important diseases, such as the symptoms induced by the bacteria associated with citrus greening disease or HLB, a very serious threat to citrus production worldwide, or of *Verticillium* wilt detection in olive orchards. Although thermal imagery has demonstrated its usefulness for early disease detection (Calderon et al. **2015**), other studies demonstrate the difficulty of applying such methods to citrus species due to seasonal changes and stomatal control of transpiration in the absence of water deficits (Gonzalez-Dugo, Zarco-

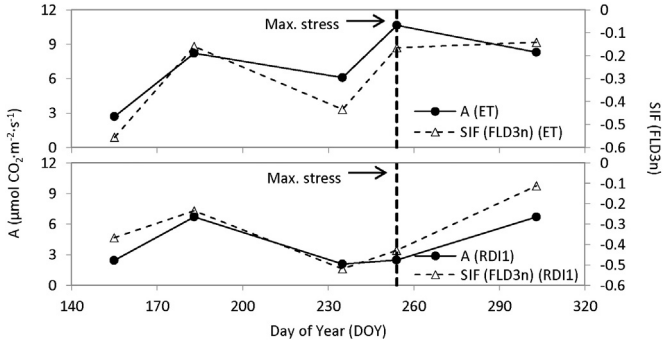

Fig. 13. Time series of the normalized SIF FLD3 (FLDn) and assimilation (A) for well-irrigated (ET) and stressed (RDI1) treatments for all flights throughout the 2013 season. Note the similar temporal behavior of SIF FLD3n and A over the season, and the differences for both A and SIF FLD3n between stressed and well-irrigated treatments at the time of maximum stress (DOY = 254).

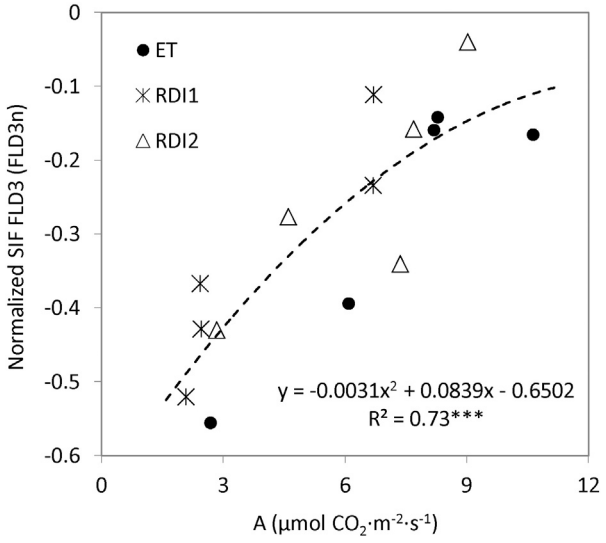

Fig. 14. Relationship between normalized SIF FLD3 (FLD3n) and assimilation (A) for all five flights during the season, for the three irrigation treatments (ET, RDI1, RDI2).

Tejada, & Fereres, **2014**). Given that most of the diseases have a direct impact on the photosynthetic apparatus, the fluorescence quantification proposed here could be a promising pre-visual indicator of diseases and other aspects of plant pathology. For this particular application, and indeed for all types of potential applications of fluorescence in precision agriculture, the resolutions needed and the actual requirements fall far from those required for global studies, in which the temporal dimension is emphasized. Under the umbrella of such different applications, the need for cost-effective sensors that are easy to operate and commercially available is critical for the successful and widespread adoption of fluorescence as a proxy for physiological status and screening in an operational context. Current widely available commercial sensors provide submeter resolutions (i.e. 20–30 cm pixel size at typical 1000 ft flight altitudes) with large sampling intervals but with the drawback of a limited spectral bandwidth which, depending on the slits used, yields resolutions ranging from 2 to 7 nm FWHM. For these reasons, a major challenge for the scientific community is to make progress on methodologies suitable for the retrieval of SIF from these hyperspectral sensors in the context of stress–detection and agronomic applications. Adapting current models and procedures to use such commercially available imagers for physiological condition assessment will open up several new avenues of research, permitting decision-making in real commercial and operational applications, as well as providing the high-resolution validation data needed for global studies and for better interpretation of fluorescence in mixed pixels and heterogeneous canopies acquired on satellite scales.

5. Conclusions

Solar-induced chlorophyll fluorescence quantified from airborne hyperspectral imagery was the most robust indicator of photosynthesis in this study, which comprised seven midday flights and two diurnal airborne experiments in 2012 and 2013. Our main conclusion is that SIF retrieved using the FLD3 method was the most statistically significant indicator of assimilation measured on all flights, showing the highest coefficient of determination of all indices calculated from the hyperspectral imagery. In particular, FLD3 performed better than structural indices (RDVI, and MTVI1) and chlorophyll indices (TCARI, TVI, CI). The only other indicator that was statistically significant throughout the season was MTVI1, although it yielded lower levels of significance than FLD3. The indicators that took both structure and chlorophyll into account, without fluorescence (RDVI or MTVI1 combined with TCARI, TVI and CI), reached lower statistical significance and correlation coefficients than fluorescence alone (FLD3). A normalization scheme proposed for the airborne-quantified fluorescence for all dates using the unstressed (well-irrigated) trees on each flight date as a reference, enabled us to generate a single relationship between normalized SIF FLD3 (FLDn) and assimilation rates for the entire growing season at both tree and treatment levels. In conclusion, the two-year experiment showed the validity of using fluorescence retrievals from broader-resolution hyperspectral imagery (i.e. spectral resolution 1–5 nm FWHM) in the context of precision agriculture and crop monitoring studies for stress-detection purposes.

Acknowledgements

The authors gratefully acknowledge the financial support of the Spanish Ministry of Science and Education (MEC) for projects AGL2012-40053-C03-01, Consolider_RIDECO, and AGL2012-35196. D. Notario, A. Vera, A. Hornero, R. Romero and M. Medina are also thanked for their technical support during the field and airborne campaigns.

References

Baldocchi, D., Falge, E., Gu, L., Olson, R., Hollinger, D., Running, S., ... Wofsy, S. (2001). FLUXNET: A new tool to study the temporal and spatial variability of ecosystem-scale carbon dioxide, water vapor, and energy flux densities. *Bulletin of the American Meteorological Society*, *82*(11), 2415–2434.

Berni, J. A. J., Zarco-Tejada, P. J., Suárez, L., & Fereres, E. (2009). Thermal and narrowband multispectral remote sensing for vegetation monitoring from an unmanned aerial vehicle. *IEEE Transactions on Geoscience and Remote Sensing*, *47*(3), 722–738.

Calderón, R., Zarco-Tejada, P. J., Lucena, C., & Navas-Cortés, J. A. (2013). High-resolution airborne hyperspectral and thermal imagery for pre-visual detection of *Verticillium* wilt using fluorescence, temperature and narrow-band indices. *Remote Sensing of Environment*, *139*, 231–245.

Calderón, R., Navas-Cortés, J. A., & Zarco-Tejada, P. J. (2015). Early detection and quantification of *Verticillium* wilt in olive using hyperspectral and thermal imagery over large areas. *Remote Sensing*, *7*, 5584–5610. http://dx.doi.org/10.3390/rs70505584.

Cogliati, S., Rossini, M., Julitta, T., Meroni, M., Schickling, A., Burkart, A., ... Colombo, R. (2015). Continuous and long-term measurements of reflectance and sun-induced chlorophyll fluorescence by using novel automated field spectroscopy systems. *Remote Sensing of Environment*, *164*, 270–281.

Damm, A., Elbers, J., Erler, E., Gioli, B., Hamdi, K., Hutjes, R., ... Rascher, U. (2010). Remote sensing of sun induced fluorescence to improve modeling of diurnal courses of gross primary production (GPP). *Global Change Biology*, *16*, 171–186.

Damm, A., Erler, A., Hillen, W., Meroni, M., Schaepman, M. E., Verhoef, W., & Rascher, U. (2011). Modeling the impact of spectral sensor configurations on the FLD retrieval accuracy of sun-induced chlorophyll fluorescence. *Remote Sensing of Environment*, *115*, 1882–1892.

Damm, A., Guanter, L., Paul-Limoges, E., van der Tol, C., Hueni, A., Buchmann, N., ... Schaepman, M. E. (2015). Far-red sun-induced chlorophyll fluorescence shows ecosystem-specific relationships to gross primary production: An assessment based on observational and modeling approaches. *Remote Sensing of Environment*, *166*, 91–105.

Daumard, F., Goulas, Y., Ounis, A., Pedrós, R., & Moya, I. (2015). Measurement and correction of atmospheric effects at different altitudes for remote sensing of sun-induced fluorescence in oxygen absorption bands. *IEEE Transactions on Geoscience and Remote Sensing*, *53*, 9.

Evain, S., Flexas, J., & Moya, I. (2004). A new instrument for passive remote sensing: 2. Measurement of leaf and canopy reflectance changes at 531 nm and their relationship with photosynthesis and chlorophyll fluorescence. *Remote Sensing of Environment*, *91*, 175–185.

Flexas, J., Bota, J., Escalona, J. M., Sampol, B., & Medrano, H. (2002). Effects of drought on photosynthesis in grapevines under field conditions. An evaluation of stomatal and mesophyll limitations. *Functional Plant Biology*, *29*, 461–471.

Frankenberg, C., Fisher, J. B., Worden, J., Badgley, G., Saatchi, S. S., Lee, J. -E., ... Yokota, T. (2011). New global observations of the terrestrial carbon cycle from GOSAT: Patterns of plant fluorescence with gross primary productivity. *Geophysical Research Letters*, *38*, L17706. http://dx.doi.org/10.1029/2011GL048738.

Gamon, J. A., Peñuelas, J., & Field, C. B. (1992). A narrow-wave band spectral index that tracks diurnal changes in photosynthetic efficiency. *Remote Sensing of Environment*, *41*, 35–44.

Goldhamer, D. A., & Fereres, E. (2001). Irrigation scheduling protocols using continuously recorded trunk diameter measurements. *Irrigation Science*, *20*, 115–125.

Gonzalez-Dugo, V., Zarco-Tejada, P. J., & Fereres, E. (2014). Applicability and limitations of using the crop water stress index as an indicator of water deficits in citrus orchards. *Agricultural and Forest Meteorology*, *198–199*, 94–104.

Guanter, L., Zhang, Y., Jung, M., Joiner, J., Voigt, M., Berry, J. A., & Griffis, T. J. (2014). Global and time-resolved monitoring of crop photosynthesis with chlorophyll fluorescence. *Proceedings of the National Academy of Sciences (PNAS)*. http://dx.doi.org/10.1073/pnas.132000811.

Gueymard, C. A. (1995). SMARTS, a simple model of the atmospheric radiative transfer of sunshine: Algorithms and performance assessment. *Technical report no. FSEC-PF-270-95*Cocoa, FL: Florida Solar Energy Center.

Gueymard, C. A. (2001). Parameterized transmittance model for direct beam and circumsolar spectral irradiance. *Solar Energy*, *71*(5), 325–346.

Gueymard, C. A., Myers, D., & Emery, K. (2002). Proposed reference irradiance spectra for solar energy systems testing. *Solar Energy*, *73*(6), 443–467.

Gueymard, C. A. (2005). Smarts code, version 2.9.5 user's manual solar consulting services. Online PDF document from http://www.nrel.gov/rredc/smarts/

Haboudane, D., Miller, J. R., Pattey, E., Zarco-Tejada, P. J., & Strachan, I. (2004). Hyperspectral vegetation indices and novel algorithms for predicting green LAI of crop canopies: modeling and validation in the context of precision agriculture. *Remote Sensing of Environment*, *90*(3), 337–352.

Hernández Clemente, R., Navarro Cerrillo, R., & Zarco-Tejada, P. J. (2014). Deriving predictive relationships of carotenoid content at the canopy level in a conifer forest using hyperspectral imagery and model simulation. *IEEE Transactions on Geoscience and Remote Sensing*, *52*(8), 5206–5217. http://dx.doi.org/10.1109/TGRS.2013.2287304.

Joiner, J., Guanter, L., Lindstrot, R., Voigt, M., Vasilkov, A. P., Middleton, E. M., ... Frankenberg, C. (2013). Global monitoring of terrestrial chlorophyll fluorescence from moderate spectral resolution near-infrared satellite measurements: Methodology, simulations, and application to GOME-2. *Atmospheric Measurement Techniques Discussions*, *6*(2), 3883–3930.

Krause, G. H., & Weis, E. (1984). Chlorophyll fluorescence as a tool in plant physiology. II. Interpretation of fluorescence signals. *Photosynthesis Research*, *5*, 139–157.

Joiner, J., Yoshida, Y., Vasilkov, A. P., Yoshida, Y., Corp, L. A., & Middleton, E. M. (2011). First observations of global and seasonal terrestrial chlorophyll fluorescence from space. *Biogeosciences*, *8*(3), 637–651.

Kuze, A., Suto, H., Nakajima, M., & Hamazaki, T. (2009). Thermal and near infrared sensor for carbon observation Fourier-transform spectrometer on the greenhouse gases observing satellite for greenhouse gases monitoring. *Applied Optics*, *48*, 6716–6733.

Larcher, W. (1994). Photosynthesis as a tool for indicating temperature stress events. In E. D. Schulze, & M. M. Caldwell (Eds.), *Ecophysiology of photosynthesis* (pp. 261–277). Berlin: Springer.

Lichtenthaler, H. K., & Rinderle, U. (1988). The role of chlorophyll fluorescence in the detection of stress conditions in plants. *CRC Critical Reviews in Analytical Chemistry*, *19*(Suppl. 1), 529–585.

Lichtenthaler, H. K. (1992). The Kautsky effect: 60 years of chlorophyll fluorescence induction kinetics. *Photosynthetica*, *27*, 45–55.

Louis, J., Ounis, A., Ducruet, J. M., Evain, S., Laurila, T., Thum, T., et al. (2005). Remote sensing of sunlight-induced chlorophyll fluorescence and reflectance of Scots pine in the boreal forest during spring recovery. *Remote Sensing of Environment*, *96*, 37–48.

Malenovsky, Z., Mishra, K. B., Zemek, F., Rascher, &. U., & Nebal, L. (2009). Scientific and technical challenges in remote sensing of plant canopy reflectance and fluorescence. *Journal of Experimental Botany*, *60*, 2987–3000.

Meroni, M., Colombo, R., & Cogliati, S. (2004). High resolution leaf spectral signature for the detection of solar induced chlorophyll fluorescence. *Proceedings of the 2nd international workshop on remote sensing of solar induced vegetation fluorescence, Montreal, Canada* 17–19 November 2004.

Meroni, M., Picchi, V., Rossini, M., Cogliati, S., Panigada, C., Nali, C., ... Colombo, R. (2008a). Leaf level early assessment of ozone injuries by passive fluorescence and PRI. *International Journal of Remote Sensing*, *29*(17), 5409–5422.

Meroni, M., Rossini, M., Picchi, V., Panigada, C., Cogliati, S., Nali, C., & Colombo, R. (2008b). Assessing steady-state fluorescence and PRI from hyperspectral proximal sensing as early indicators of plant stress: The case of ozone exposure. *Sensors*, *8*, 1740–1754.

Meroni, M., Rossini, M., Guanter, L., Alonso, L., Rascher, U., & Colombo, R. (2009). Remote sensing of solar-induced chlorophyll fluorescence: Review of methods and applications. *Remote Sensing of Environment*, *113*, 2037–2051.

Meroni, M., Busetto, L., Colombo, R., Guanter, L., Moreno, J., & Verhoef, W. (2010), Performance of spectral fitting methods for vegetation fluorescence quantification. Remote Sensing of Environment, 114, 363–374 (2010).

Miller, J. R., Berger, M., Alonso, L., Cerovic, Z., Goulas, Y., Jacquemoud, S., ... Zarco-Tejada, P. J. (2004). Progress on the development of an integrated canopy fluorescence model, 2003. *International geoscience and remote sensing symposium, igarss'03. 1*. (pp. 601–603) Toulouse (France), 21–25/7 /2004. ISBN 0-7803-7929-2-0-7803-7930-6.

Moriana, A., Villalobos, F. J., & Fereres, E. (2002). Stomatal and photosynthetic response of olive (*Olea europaea* L.) leaves to water deficits. *Plant, Cell and Environment*, *25*, 395–405.

Moya, I., Camenen, L., Evain, S., Goulas, Y., Cerovic, Z. G., & Latouche, G. (2004). A new instrument for passive remote sensing 1. Measurements of sunlight-induced chlorophyll fluorescence. *Remote Sensing of Environment*, *91*, 186–197.

Naumann, J. C., Young, D. R., & Anderson, J. E. (2008). Leaf chlorophyll fluorescence, reflectance, and physiological response to freshwater and saltwater flooding in the evergreen shrub, *Myrica cerifera*. *Environmental and Experimental Botany*, *63*, 402–409.

Nichol, C. J., Rascher, U., Matsubara, S., & Osmond, B. (2006). Assessing photosynthetic efficiency in an experimental mangrove canopy using remote sensing and chlorophyll fluorescence. *Trees*, *20*, 9–15.

Papageorgiou, G. (1975). Chlorophyll fluorescence: An intrinsic probe of photosynthesis. In Govindjee (Ed.), *Bioenergetics of photosynthesis* (pp. 319–371). New York: Academic Press.

Pérez-Priego, O., Zarco-Tejada, P. J., Sepulcre-Cantó, G., Miller, J. R., & Fereres, E. (2005). Detection of water stress in orchard trees with a high-resolution spectrometer through chlorophyll fluorescence in-filling of the O_2-A band. *IEEE Transactions on Geoscience and Remote Sensing*, *43*, 2860–2869.

Plascyk, J. A., & Gabriel, F. C. (1975). The Fraunhofer line discriminatorMKII — An airborne instrument for precise and standardized ecological luminescence measurement. *IEEE Transactions on Instrumentation and Measurement*, *IM-24*, 306–313.

Porcar-Castell, A., Tyystjärvi, E., Atherton, J., van der Tol, C., Flexas, J., Pfündel, E. E., ... Berry, J. A. (2014). Linking chlorophyll a fluorescence to photosynthesis for remote sensing applications: Mechanisms and challenges. *Journal of Experimental Botany*, *65*(15), 4065–4095. http://dx.doi.org/10.1093/jxb/eru191 2014.

Quemada, M., Gabriel, J. L., & Zarco-Tejada, P. J. (2014). Airborne hyperspectral images and ground-level optical sensors as assessment tools for maize nitrogen fertilization. *Remote Sensing*, 2940–2962. http://dx.doi.org/10.3390/rs6042940 ISSN 2072-4292.

Rascher, U., Agati, G., Alonso, L., Cecchi, G., Champagne, S., Colombo, R., ... Zaldei, A. (2009). CEFLES2: The remote sensing component to quantify photosynthetic efficiency from the leaf to the region by measuring sun-induced fluorescence in the oxygen absorption bands. *Biogeosciences Discussions*, *6*(7), 2217–2266.

Roccuzzo, G., Villalobos, F. J., Testi, L., & Fereres, E. (2014). Effects of water deficits on whole tree water use efficiency of orange. *Agricultural Water Management*, *140*, 61–68.

Schaefer, K., et al. (2012). A model-data comparison of gross primary productivity: Results from the North American carbon program site synthesis. *Journal of Geophysical Research*, *117*, G03010. http://dx.doi.org/10.1029/2012JG001960.

Rossini, M., Nedbal, L., Guanter, L., Ač, A., Alonso, L., Burkart, A., ... Rascher, U. (2015). *Geophysical research letters, red and far red sun-induced chlorophyll fluorescence as a measure of plant photosynthesis, 1632–1639. http://dx.doi.org/10.1002/2014GL062943*.

Schreiber, U., & Bilger, W. (1987). Rapid assessment of stress effects on plant leaves by chlorophyll fluorescence measurements. In J. D. Tenhunen, & E. M. Catarino (Eds.), *Plant response to stress* (pp. 27–53). Berlin, Germany: Springer-Verlag.

Schreiber, U., Bilger, W., & Neubauer, C. (1994). Chlorophyll fluorescence as a nonintrusive indicator for rapid assessment of in vivo photosynthesis. In E. D. Schulze, & M. M. Caldwell (Eds.), *Ecophysiology of photosynthesis. Ecological studies. 100*. (pp. 49–70). Berlin Heidelberg New York: Springer.

Suárez, L., Zarco-Tejada, Pablo J., Sepulcre-Cantó, G., Pérez-Priego, O., Miller, J. R., Jiménez-Muñoz, J. C., & Sobrino, J. A. (2008). Assessing canopy PRI for water stress detection with diurnal airborne imagery. *Remote Sensing of Environment*, *112*, 560–575.

Suárez, L., Zarco-Tejada, P. J., Berni, J. A. J., González-Dugo, V., & Fereres, E. (2009). Modelling PRI for water stress detection using radiative transfer models. *Remote Sensing of Environment*, *113*, 730–744.

Van der Tol, C., Verhoef, W., Timmermans, J., Verhoef, A., & Su, Z. (2009a). An integrated model of soil-canopy spectral radiances, photosynthesis, fluorescence, temperature and energy balance. *Biogeosciences*, *6*, 3109–3129.

Van der Tol, C., Verhoef, W., & Rosema, A. (2009b). A model for chlorophyll fluorescence and photosynthesis at leaf scale. *Agricultural and Forest Meteorology*, *149*(1), 96–105.

Verrelst, J., Rivera, J. P., van der Tol, C., Magnani, F., Mohammed, G., & Moreno, J. (2015). Global sensitivity analysis of the SCOPE model: What drives simulated canopy-leaving sun-induced fluorescence? *Remote Sensing of Environment*, *166*, 8–21.

Villalobos, F. J., Testi, L., & Moreno-Perez, M. F. (2009). Evaporation and canopy conductance of citrus orchards. *Agricultural Water Management*, *96*(4), 565–573.

Zarco-Tejada, P. J., Berjón, A., López, R., Miller, J. R., Martín, P., & González, M. R. (2005). Assessing vineyard condition with hyperspectral indices: Leaf and canopy reflectance simulation in a row-structured discontinuous canopy. *Remote Sensing of Environment*, *99*, 271–287.

Zarco-Tejada, P. J., González Dugo, V., & Berni, J. A. J. (2012). Fluorescence, temperature and narrowband indices acquired from a UAV platform for water stress detection using a micro-hyperspectral imager and a thermal camera. *Remote Sensing of Environment*, *117*, 322–337.

Zarco-Tejada, P. J., Guillén-Climent, M. L., Hernández-Clemente, R., Catalina, A., González, M. R., & Martín, P. (2013a). Estimating leaf carotenoid content in vineyards using high resolution hyperspectral imagery acquired from an unmanned aerial vehicle. *Agricultural and Forest Meteorology*, *171–172*, 281–294.

Zarco-Tejada, P. J., Suárez, L., & González-Dugo, V. (2013b). Spatial resolution effects on chlorophyll fluorescence retrievals in a heterogeneous canopy using hyperspectral imagery and radiative transfer simulation. *Geoscience and Remote Sensing Letters*. http://dx.doi.org/10.1109/LGRS.2013.2252877.

Zarco-Tejada, P. J., Morales, A., Testi, L., & Villalobos, F. J. (2013c). Spatio-temporal patterns of chlorophyll fluorescence and physiological and structural indices acquired from hyperspectral imagery as compared with carbon fluxes measured with eddy covariance. *Remote Sensing of Environment*, *133*, 102–115.

Zarco-Tejada, P. J., Catalina, A., González, M. R., & Martín, P. (2013d). Relationships between net photosynthesis and steady-state chlorophyll fluorescence retrieved from airborne hyperspectral imagery. *Remote Sensing of Environment*, *136*, 247–258.